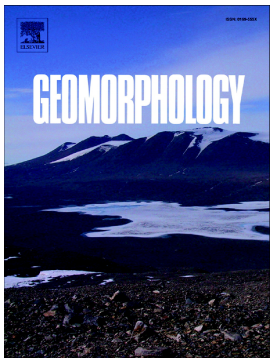

Controls on the erosion of the continental margin of southeast Brazil from cosmogenic 10Be in river sediments

Daniel H. de Souza, Finlay M. Stuart, Ángel Rodés, Fabiano N. Pupim, Peter C. Hackspacher

PII: S0169-555X(19)30027-3
DOI: https://doi.org/10.1016/j.geomorph.2019.01.020
Reference: GEOMOR 6654

To appear in: *Geomorphology*

Received date: 2 July 2018
Revised date: 25 January 2019
Accepted date: 30 January 2019

Please cite this article as: D.H. de Souza, F.M. Stuart, Á. Rodés, et al., Controls on the erosion of the continental margin of southeast Brazil from cosmogenic 10Be in river sediments, Geomorphology, https://doi.org/10.1016/j.geomorph.2019.01.020

Controls on the erosion of the continental margin of southeast Brazil from cosmogenic ^{10}Be in river sediments

Daniel H.de Souza[1*], Finlay M. Stuart[2], Ángel Rodés[2], Fabiano N. Pupim[3] and Peter C. Hackspacher[1]

[1]Instituto de Geociências e Ciências Exatas, Universidade Estadual Paulista, Avenida 24A, 1515, CEP 13506-900, Rio Claro, Brazil.

[2]Scottish Universities Environmental Research Centre, Rankine Avenue, East Klibride G75 0QF, United Kingdom

[3]Departamento de Ciências Ambientais, Universidade Federal de São Paulo, Rua São Nicolau, 210, 09913-030, Diadema, Brazil.

[*]Author for communication:

Cell: +55 19 988832967. E-mail: danieudani@yahoo.com.br

ABSTRACT

The Atlantic Ocean coast region of southeast Brazil contains two coast-parallel mountain ranges (the Serra do Mar and Serra da Mantiqueira) generated by tectonic activity pulses tens of millions years after the main continental rift event occurred around 120 Ma. Although the short-term erosion rates for the region are established, the relative importance of the factors controlling erosion is poorly constrained. We combine new and published catchment-averaged erosion rates (n=48) using *in situ*-produced ^{10}Be concentrations in quartz from river sediments to establish the regional erosion pattern. The river catchments are (i) escarpment topography, (ii) high-altitude low-relief and (iii) mixed topography, which record how escarpment fronts are migrating inland. Ocean-facing coastal escarpment catchments of the Serra do Mar (ε = 18–53 m/Ma) can be eroded approximately twice as fast as continent-facing escarpment catchments in the Serra do Mar and Serra da Mantiqueira (ε = 7–24 m/Ma). The correlation between the normalized channel steepness index (k_{sn}) and slope angle indicates that river incision and hillslope erosion processes combine to maintain the high relief. The Serra do Mar catchments define a mean slope angle threshold indicating that landslides are the dominant erosional process when slope angles in excess of ~30°. Tectonic activity is low and plays no significant role in driving erosion. A first-order relationship between erosion rate and precipitation-temperature across the region implies that climate plays a key role in soil production, river incision and in triggering erosional processes. Although the high topographic relief is a pre-condition for the occurrence of significant erosion, the climatic condition is the outlining factor of the regional variation in erosion rates.

Keywords: Serra do Mar, Serra da Mantiqueira, escarpment retreat, passive margin.

1. Introduction

It has been debated for decades how high relief landscapes are maintained at mature passive margins (e.g., Summerfield, 1991). Flexural isostasy, where continent erosion and offshore basins sediment deposition produce constant uplift and subsidence after rifting ceases, has emerged as the prevailing hypothesis (Summerfield, 1991; Braun et al. 2014). The development of *in situ* cosmogenic nuclides has provided quantitative estimates of the denudational history of many passive margins and allowed this hypothesis to be tested.

In situ-produced cosmogenic ^{10}Be measured in bedrock and river catchments show that present day erosion rates are low, and they do not exceed few tens of meters per million years (e.g. Bierman and Caffee, 2001; Matmon et al. 2002). This is consistent with the long-term record derived from low temperature thermochronology (e.g. Persano et al., 2002). Cosmogenic ^{10}Be-derived erosion rates of river catchments in Sri Lanka (Vanacker et al., 2007), Australia, (Heimsath et al., 2009; Nichols et al., 2014), southeastern United States (Sullivan, 2007), southern India (Mandal et al., 2015) and western Brazil (Salgado et al., 2016; Gonzalez et al., 2016) are lower than during the rift stages. However, there is significant variation in erosion rate between and within regions that reflects the role played by factors other than tectonics.

A global dataset presented by Portenga and Bierman (2011) has highlighted the influence of climate on erosion rates; polar and arid zones yielding the highest and lowest rates respectively. For passive margins, this reflects in the difference between arid zones, such as Namibia, where erosion rates are low (~10 m/Ma; Bierman and Caffee, 2001), and the humid zones, such as southern India, where the escarpment zones erode more rapidly (~50 m/Ma; Mandal et al., 2015). Rock resistance (Scharf et al., 2013; Pupim et al., 2015) and geological structure may control the escarpment evolution in places (Gunnell and Harbor, 2010), since they can define escarpment position and point of river captures that lead to the escarpment retreat. The previous topographic relief appears to have a feedback relationship with erosion rates, given the overall strong correlation between erosion rate and morphometric parameters in several scales (Portenga and Bierman, 2011). Numerical models of high-elevation passive margin evolution have demonstrated that incising bedrock channels and the high relief between the escarpment top and base level ensure that erosion and transport efficiency lead to the generation and maintenance of high-relief and the long-term escarpment retreat (Tucker and Slingerland, 1994). These studies suggest there is a complex interaction between the factors that control erosion.

Several studies have reported ^{10}Be-derived erosion rates in southern and southeastern Brazil (Salgado et al, 2008, 2014, 2016; Cherem et al., 2012; Rezende et al.; 2013; Barreto et al, 2014; Gonzales et al., 2016, Sordi et al., 2018). Some have highlighted the local role of the lithology in controlling erosion (Salgado et al, 2008; Rezende et al, 2013). However, morphological characteristics measured by parameters such as mean local relief and mean

slope have shown to be the main control on the erosion rates in regional scale studies (Salgado et al, 2016; Gonzalez et al., 2016). The role of climate is largely ignored, although Gonzalez et al. (2016) demonstrated locally a good correlation between average catchment erosion rates and mean annual precipitation that is not borne out by the regional dataset.

In this paper, we focus on the central part of the continental margin of southeastern Brazil (Fig. 1). Reactivation of Precambrian shear zones in the Upper Cretaceous to Paleogene has created two coast-parallel mountain ranges, the Serra do Mar and Serra da Mantiqueira (Almeida and Carneiro, 1998; Cobbold et al., 2001) (Fig.1A and 2). The mountains are prominent topographic barriers and generate significant precipitation and temperature variation over short distances (Sant'Anna Neto, 2005). The low intensity tectonism makes the region a useful natural laboratory for studying the inter-relationship of relief, climate, geology and erosion. We report new ^{10}Be-derived mean erosion rates from eighteen catchments from geomorphically-distinct regions. New erosion rate and nearby catchments data (Salgado et al., 2016) are combined with morphometric, climatic and geologic parameters in order to evaluate the main drivers of erosion and to determine their relative role in the escarpment evolution of an high-elevation passive margin landscape under humid tropical climate. Thus, we aim to constrain the potential climatic influence on erosion rates, considering the topographic relief variability as well as the interaction between river incision and hillslope processes.

2. Study region

The river catchments studied here are in a region between São Paulo and Rio de Janeiro (Fig. 1B) in southeastern Brazil. The region is a mature passive margin that includes two coast-parallel mountain ranges (the Serra do Mar and Serra da Mantiqueira) separated by a 15–20 km wide rift valley. Serra do Mar rises steeply from the Atlantic Ocean coastal plain to reach a plateau at ~1,500 m above sea level. It is separated from Serra da Mantiqueira (up to 2,800 m) by NE-SW trending basins that are filled with up to 800 m of Tertiary clastic sediments through which Paraíba do Sul river flows (Ricommini et al., 2004) (Fig. 1 and 2). The Atlantic Ocean facing slopes of both mountain ranges have prominent escarpments. The upland areas of both mountain belts are generally of low relief, except for the Itatiaia plateau in Serra da Mantiqueira (Fig. 2B) which is deeply dissected (Radam Brasil, 1983). Thick regolith (up to 40 m, including saprolite and soil) mantles most of the upland landscape (e.g. Modenessi-Gautierri et al. 2011). Exposed bedrock is common on the escarpments where the regolith is typically thin (Furian et al., 1999). The regional bedrock is Precambrian gneiss and granites in Mantiqueira province (Fig. 1B) (Heilbron et al., 2004). Quartz-bearing rocks are uniformly distributed throughout these catchments.

The topography is the result of tectonic reactivation of Precambrian shear zones that occurred several 10’s of millions of years after the rifting of the Gondwana supercontinent and Atlantic Ocean opening during late Jurassic to early Cretaceous (Zalán, 2004). The offshore sediment record suggests that the margin was subjected to a major pulse of rock uplift during the Late Cretaceous (Almeida and Carneiro, 1998; Zalán and Oliveira, 2005). This is consistent with

the cooling history of the continental margin determined by low temperature thermochronology (Gallagher et al., 1994; Hackspacher et al., 2004; Hiruma et al., 2010, Cogné et al. 2011). This fact coincided with the intrusion of several alkaline bodies, mainly along the WNW-ESE trending Poços de Caldas–Cabo Frio alignment (Thomaz-Filho et al. 2005) (Fig. 1B). The topography of the Serra do Mar and Serra da Mantiqueira was established during a phase of crustal extension in the Paleogene that led to the formation of the São Paulo, Taubaté and Resende basins that separate the two mountain ranges (Fig. 1B, 2A and B) (Ricommini et al., 2004). The basin underwent a phase of deformation in the Neogene in response to a regional compressive stress regime (Riccomini and Assumpção, 1999; Ricommini et al., 2004). Despite the relatively recent tectonic activity, the current earthquake frequency (Assumpção, 1998) and low peak ground acceleration below 1g (Gonzalez et al., 2016) indicate that the region is experiencing only low tectonic activity.

The regional topography has a direct influence on atmospheric circulation, defining the local climate. The easterly winds of Atlantic Tropical Mass in the Summer and South Polar Anticyclone in the Winter, change humidity and temperature when they meet the topographic barriers of the Serra do Mar and Serra da Mantiqueira (Sant'Anna Neto, 2005). Mean annual precipitation reaches 3,000 and 2,000 mm at Serra do Mar and Serra da Mantiqueira escarpments respectively, with no dry months, and mean annual temperatures below 15°C. The mean annual precipitation is around 1,500 mm and the mean annual temperature is 21°C in Paraíba do Sul Valley (Radam Brasil, 1983).

Montane Atlantic forests occur in regions of high precipitation; while the semi-deciduous seasonal vegetation prevails in the drier, low elevation Paraíba do Sul valley. Grasslands and araucaria forests are also common in high altitudes and low temperature regions (Radam Brasil, 1983). Species distribution models (Leite et al., 2016) suggest the persistence of the humidity and expansion of the forest to continental shelf during the last glacial cycle (Pessenda et al., 2009, Cruz et al., 2009, Pivel et al., 2010). Similar environmental conditions are likely to have persisted at least in the escarpment zones over the time recorded by the cosmogenic ^{10}Be in this study. In the highlands, episodic erosional pulses are evident in colluvium deposits in Campos do Jordão, Itatiaia and Bocaina plateau (Hiruma et al., 2013). These may be related to millennial and orbital climatic oscillations and consequent local expansion and shrinkage of forests (Cruz et al., 2009).

3. Methods

3.1. ^{10}Be-derived catchment erosion rates

We have measured mean erosion rates from ^{10}Be concentrations in quartz from catchments in three geomorphically-distinct regions of Serra do Mar (Fig. 1, 2 and 3): (i) the coastal escarpment of Serra do Mar (SM) (Fig. 2A and 3A); (ii) the Serra do Quebra-Cangalha (SQC), a series of SW-NE trending hills at the northwest end of Serra do Mar (Fig. 2A and 3B); and (iii) Bocaina plateau (Boc), a tilted mountain block at the northeastern end of Serra do Mar (Fig. 2B and 3C). Catchments have been sampled from two regions in Serra da Mantiqueira: (i) the Campos do Jordão plateau (CJ), a low relief upland in the

southwest that is drained by rivers along Precambrian shear zones (e.g. Sapucaí river valley) (Fig. 2A, C and 3D); and (ii) Itatiaia plateau (Ita), an upland at the northeast end of the region that includes Late Cretaceous intrusive alkaline bodies (Fig. 2B, C and 3E), although all catchments in the Itatiaia plateau are completely in the Precambrian basement.

The river catchments are classified into three types: those dominated by (i) escarpment topography, (ii) high-altitude catchments that are dominantly low-relief (which we term *highland*) and (iii) catchments with mixed topography (Table 2). Samples of sand were collected from the active channels in eighteen river catchments. The catchments range from 12 to 77 km^2. Smaller catchments were not sampled in order to avoid the influence of recent mass movements. Naturally vegetated catchments, including conservation areas, were sampled in order to avoid anthropogenic influence. Wherever possible, samples were collected from paired catchments that shared a topographic divide; one river draining the escarpment to the ocean and another one draining the upland region.

The sand samples were prepared in the Department of Petrology and Mineralogy, São Paulo State University, Rio Claro, Brazil. We sieved sediment samples and isolated the 250-500 μm fraction. After the removal of magnetic grains, each sample was etched with diluted hydrofluoric and nitric acids to remove minerals other than quartz. The quartz chemistry was performed at Scottish Universities Environmental Research Centre. The quartz fraction was digested three times with hydrofluoric acid to dissolve ~30% of the quartz. The purity of the fraction was tested by ICP-OES, and in all cases Al concentrations were lower than 150 ppm. This quartz fraction was dissolved in concentrated

hydrofluoric acid together with ~240 µg of ^{9}Be spike carrier. The acid was evaporated and the residue re-dissolved in hydrochloric acid. Anion (2 ml AG-1 X8 200-400# resin column) and cation (2 ml AG-50 X8 200-400# resin column) chromatography were used to isolate the beryllium, which was then precipitated as a hydroxide and transformed to oxide at 900ºC. Samples were mixed with niobium (BeO:Nb ~1:6) and mounted in copper AMS targets. ^{10}Be/Be ratios were measured at SUERC with 5 MV Pelletron accelerator mass spectrometer (Xu et al. 2010). ^{10}Be concentrations were calculated using ^{10}Be/Be ratio of 2.79 x 10^{-11} for the NIST SRM4325 standard. The processed blank ratios were between 0.1 and 7.1% of the sample ^{10}Be/Be ratios. The uncertainty of this correction is included in the standard uncertainties.

Production rates were calculated for each cell in the 30 m resolution digital elevation data from the Shuttle Radar Topography Mission (SRTM DEM) (Farr et al., 2007) using Stone (2000) scale factors, and then the production-rate weighted average elevation for individual catchment was estimated. Shielding factors were calculated from the SRTM DEM using the formulation of Codilean (2006). The ^{10}Be concentrations, shielding factor and production rates of the new samples are shown in Table 1. Catchment-averaged erosion rates (ε; Table 2) were calculated with CRONUS-Earth online calculators MATLAB code (Balco et al., 2008, version 2.3, June, 2016) with time-independent Lal/Stone scheme. ^{10}Be concentrations from an additional twenty-eight river sediment samples, reported by Salgado et al. (2016), from adjacent catchments were integrated in our analysis (Table S1 and Figure 4). Erosion rates for all catchments were calculated via the scheme developed for our samples (Table 2).

3.2. Morphometric parameters

All morphometric parameters were based on a 30 m resolution SRTM DEM (Farr et al., 2007; available at http://earthexplorer.usgs.gov/) and calculated by TopoToolbox 2 (Schwanghart and Scherler, 2014). Slope angles for each pixel in the DEM were computed as the dip of a plane fit to a 3x3 pixel array centered on the pixel of interest. For each catchment slope the values of all pixels were averaged.

Local relief (LR) was calculated for each pixel in the DEM and averaged in each catchment. The LR of each pixel used the elevation range within a circular window with radii ranging from 100 m to 5 km (Montgomery and Brandon, 2002; DiBiase et al., 2010) (Table S2). This metric describes landscape steepness on different scales. In general terms, LR measured at smallest radii is a proxy for hillslope angle. As the radii increases, the LR records the relief of successively larger tributary catchments. Thus, the largest radius records the main channel relief of the catchment (Montgomery and Brandon, 2002; DiBiase et al., 2010). For small catchments and radii >3 km, the local relief calculations incorporate topography outside the catchment. At this scale the total catchment relief (CR), the simple catchment range height, is a better metric and is also considered in the analysis.

The channel steepness index (k_s) was used to determine the relationship between river relief and erosion rate. It describes a river longitudinal profile from the relation between local slope (S) and upstream area (A) (Flint, 1974):

$$S = k_s A^{-\Theta} \quad (1)$$

where Θ is the concavity index. Since variation of the best-fit for Θ is common and strongly correlated to k_s, the channel steepness index was normalized (k_{sn}) through a fixed reference concavity of Θ_{ref} = 0.45 (Wobus et al., 2006; Ouimet et al., 2009). The k_{sn} calculation with TopoToolbox 2 (Schwanghart and Scherler, 2014) is performed via the following steps: flow direction and flow accumulation definition in the DEM; drainage network definition; gradient calculation for the stream segments; and k_{sn} calculation. k_{sn} values in stream segment length of 300 meters have been calculated assuming that the channels occupy cells that have a minimum upslope area of 1.8×10^5 m².

3.3. Climatic and rock resistance parameters

Mean annual precipitation (MAP) from 1977 to 2006 (at http://www.cprm.gov.br/publique/Hidrologia/Mapas-e-Publicacoes/Atlas-Pluviometrico-do-Brasil-1351.html) and mean annual temperature (MAT) from 1960 to 2000 (Hijmans et al., 2005; Fick and Hijmans, 2017; http://www.worldclim.org/) were used as a proxy for modern climate (Figure S1). Weather stations are distributed along the entire study area, ensuring that the first order climatic variability across the region is recorded (Fig. S1A). However, as the stations are not evenly distributed across the study area, there is a degree of uncertainty between catchments within the same sector (highland or escarpment) in some geomorphic regions. k_{sn} (section 3.2) has been calculated by replacing the drainage area with discharge (Bookhagen and Strecker, 2012), based on precipitation. This was done by a D8 routing scheme where it is assumed that all water flows down the steepest path (Bookhagen and Strecker,

2012). The resolution of the MAP data is insufficient for a detailed catchment-scale analysis (and we do not account for evapo-transpiration and groundwater loss). Thus, the MAD is a simple proxy for the purpose of comparison and testing the potential climatic influence on incision.

In order to determine the proportion of distinct rock types in the river catchments we have used the 1:100,000 geologic maps: Pouso Alto (Pedrosa Soares et al., 2003), Volta Redonda (Heilbron et al, 2007), Itajuba (Trouw et al., 2008), Campos do Jordão (Peternel et al., 2014) and Pindamonhangaba (Trouw et al., 2014). Where maps at this scale are not available, we used Santos geologic map at 1:250.000 scale (Morais, 1999), Rio de Janeiro state geologic map at 1:400,000 (Heilbron et al, 2016) and São Paulo State geologic map at 1:750,000 scales (Perrota et al, 2005). We measured all variables in the entire study area, including catchments sampled for ^{10}Be analysis by Salgado et al. (2016).

4. Results and data analysis

4.1. Catchment-averaged erosion rates

Erosion rates range from 5.2 ± 0.5 to 53.3 ± 4 m/Ma (average = 16 ± 11 m/Ma) and they are integrated over periods between 11 and 115 ka (Table 2). These new erosion rates are broadly consistent with the rates reported for nearby catchments presented by Salgado et al. (2016) (Fig. 4).

The highland catchments in this study have the lowest erosion rates, ranging from 5.2 ± 0.5 m/Ma to 15.6 ± 1.3 m/Ma (n=23). The highland catchments with the highest erosion rates (> 10 m/Ma, n=7) are mainly found in Itatiaia and Campos do Jordão plateau and are dominated by incised rivers

(e.g. catchments E3, E5, E7, E8 and P20). The ocean-facing escarpment and mixed topography catchments in Serra do Mar have the highest erosion rates in the region (18.7 ± 1.8 m/Ma to 53.3 ± 4 m/Ma, n=7). The average (34.7 ± 11.25 m/Ma) is twice the average of escarpment catchments in the other regions (16.6 ± 4.9 m/Ma, n = 17). In Campos do Jordão plateau the escarpment and mixed catchments erode at between 7.1 ± 0.6 and 23.9 ± 1.9 m/Ma (n=3). This is similar to the erosion rates of Itatiaia plateau (11.1 ± 1 to 23.5 ± 2 m/Ma, n=7) and the continent-facing regions in Serra do Mar: Bocaina plateau and Quebra-Cangalha (10.3 ± 0.9 to 22.9 ± 2.3 m/Ma, n=7) (Table 2 and Fig.4).

4.2. Inter-relationships between the topographic parameters

The mean slope angles of the catchments are between 11° and 25°, and the normalized channel steepness index (k_{sn}; considering drainage area) ranges from 18 $m^{0.9}$ to 119 $m^{0.9}$ (Table 2). There is a strong correlation between these two parameters (Fig 5A) that indicates a general correspondence between river incision and hillslopes erosion processes.

Mean local relief measured at several scales (Table S2) allows a detailed evaluation of the hillslope and drainage network relief behavior. Local relief is strongly correlated with slope angle at radii up to 1 km (Fig. 5B), which implies that the relationship holds for tributary catchments that are less than 3 km^2. In contrast, k_{sn} is well correlated with local relief at radii between 1 and 2.5 km. This difference distinguishes slope angle from the k_{sn} behavior, although they correlate well with each other. This difference can be understood from the analysis of the relationship between LR radii and catchment type. There is a discontinuous increase in LR with radii in mixed catchments that are not

apparent in the other catchment types (Fig. 5C-F). That k_{sn} matches LR at radii of 1–2.5 km likely reflects the effect of the mixed catchment topography. The mixed catchments tend to have higher k_{sn} values, plotting below the best-fit line in Figure 5A.

4.3. Correlation between erosion rate and topographic parameters

4.3.1. Mean local relief

A linear correlation between mean local relief and erosion rate exists until radii of 2.5 km (Fig. 5b), which implies a relation with both hillslope (slope angle) and river relief (k_{sn}). Erosion rate is better correlated with total catchment relief (CR) than LR at radii higher than 3 km due the effect of outside catchment areas in the measurement. However, the correlation is weaker than with LR at radii < 2.5 km. At the scale of CR, the mixed catchments reach the maximum relief increase in relation to the other catchment types (Fig. 5F); thus, erosion rates are not readily sensitive to this relief increase.

4.3.2. Mean slope angle

Across the region catchment erosion rates below ~20 m/Ma appear to be positively correlated with slope angle (S) up to 25° (Fig. 6A). Slope angles of escarpment and mixed catchment in Serra do Mar do not exceed 25° while erosion rates in the high slope catchments can be up to 53 m/Ma, giving the correlation an asymptotic form. Assuming that the slope angle approaches the threshold (Montgomery, 2001), we have modeled the morphological transition from slope-dependent to threshold hillslopes, creating a proxy for erosion rate.

For that, we have based in soil transport laws that account for both creep-related and landslide processes (Roering et al., 1999; DiBiasi et al., 2010):

$$\varepsilon = AS + BS / (1 - (S/S_c)^2) \quad (2)$$

where S is slope, S_c is a critical slope at which soil flux approaches infinity, A is the linear correlation between S and ε, and B is a transitional coefficient between slope-dependent (A) to threshold (S_c). We have calculated coefficients by inverse modeling from the relation between erosion rates and slope angle. The best fit for the model yields $S_c = 30°$ (Fig. 7A) (Supplementary data 2A).

4.3.3. Normalized channel steepness

The correlation between erosion rate and normalized channel steepness (k_{sn}) reveals a trend that reaches a threshold for k_{sn} values that is more pronounced than slope angle (Fig. 6B). Although river erosion processes (abrasion and plucking) are unlike those of hillslope processes, they include a critical threshold that, when exceeded, strongly influences long-term erosion rates (Wipple, 2004). Consequently, equation (2) can be adapted to describe the transition to the threshold zone for river incision (Supplementary data 2B). The contributing area, which gives the river incision its advective nature, is already included in k_{sn} index (equation 1):

$$\varepsilon = Ak_{sn} + Bk_{sn} / (1 - (k_{sn}/k_{snc})^2) \quad (3)$$

where k_{snc} is a critical k_{sn} value, A is the linear correlation between k_{sn} and ε, and B is a transition coefficient between k_{sn}-dependent erosion rates to the threshold zone (k_{snc}). The threshold zone is largely defined by the Serra do Mar catchments and the transition is more abrupt than for slope angles (Fig. 6B), indicating that hillslopes are still adapting to incision. Replacing drainage area with discharge in the k_{sn} calculation amplifies the importance of the high k_{sn} Serra do Mar catchments. This is best adjusted with model (3) (Fig. 6C) (Supplementary data 2C) and indicates that the precipitation gradient across the region plays a key role in the river incision and, consequently, in the higher erosion rates of Serra do Mar catchments.

4.4. Lithological and climatic influence on erosion rates

There is no clear relationship between erosion rate and lithology (Fig. 7). For instance, where catchments have a range of lithologies, e.g. the low relief highland catchments, there is no apparent correlation with erosion. In the more rapidly eroding escarpment catchments, the gneiss- and schist-dominated catchments appear to erode slightly faster than the granite catchments (see Itatiaia and Bocaina catchments). However, the high erosion rates in Serra do Mar have no clear relation to lithology.

Erosion rate is moderately correlated with the proxies for climate. For instance, the high erosion rates in the Serra do Mar catchments coincide with high mean annual precipitation (MAP; Fig. 8A) and mean annual temperature (MAT; Fig. 8B). However, this relationship is not observed throughout the region. For instance, the high MAP of the Itatiaia plateau and high MAT of the Bocaina plateau coincide with catchment-averaged erosion rates that are

significantly lower than those in the Serra do Mar catchments (Fig. 8A & B). To evaluate the influence of climate factors on erosion rates we have integrated MAP and MAT with a least-square multiple linear regression between erosion rates, MAP and MAT. Least-square linear regressions yield R^2 = 0.65 and p-values of 5.4×10^{-6} for MAP and 1.7×10^{-7} for MAT, attesting to the possibility that both could regulate erosion rates (Supplementary data 2E). In Figure 8C the measured erosion rates are plotted against those determined by the regression-derived model. The generally good fit implies that climatic factors provide a first order control on erosion rate across the region. While it does not fully explain the erosion rate variation, it clearly influences the differences between the geomorphological regions.

5. Discussion

5.1. Escarpment evolution

On the continental margin of southeastern Brazil, drainage channels and hillslopes are adjusted to each other in the low-relief highland and step escarpment catchments (Fig. 5A). Topographically mixed catchments are in a temporary imbalance and represent a transition from a highland area to an escarpment zone. It starts from episodic capture of a highland catchment by an escarpment river, promoting the inland migration of the escarpment front. This escarpment evolution pattern has been recognized in several passive margins (Gunnel and Harbor, 2010) including neighboring areas in south and southeastern Brazil (Cherem et al., 2012; Salgado et al., 2016; Sordi et al., 2018). Figure 9 illustrates this process using the long-river profiles of three catchments at different stages of the evolution: P24, P30 and P27. The scatter

in the slope-area plots decreases from P24 to P27, demonstrating the temporal adjustment of the drainage segments towards the final state (Wobus et. al., 2006).

In the Campos do Jordão plateau, several recent river capture events have been identified (Modenesi-Gauttierri et al., 2002), for example the P24 catchment (Fig. 3D and 9A). The capture promotes an instantaneous increase in the total catchment relief (see Fig. 5. C-F). However, the characteristics of the pre-existing catchment (channel steepness, hillslope angle and local relief) are preserved above and below the knickpoint. Small tributaries at the knickpoint seem to increase relief relative to the main river course (Fig. 9A). The preserved highland segment represents ~65% of the total area of the P24 catchment (Fig. 3D and 9A). Given the high ^{10}Be concentration in the sediments before the capture, the mean erosion rate of the catchment as a whole is reduced and stays close to typical value for highlands catchments (Fig. 4), confirming that the increase in catchment relief is not generally reflected in the erosion rate. This has been reported by Cherem et al. (2012) in Serra da Mantiqueira, northeast of the study area, and by Mandal et al. (2015) in southern India.

In Serra do Mar, P30 is perhaps the most mature catchment of those studied (Fig. 3A and 9B). The river profile suggests that several capture events have occurred in the recent past. This is most evident in section P30d, subdued in P30a and not apparent in P30c. Overall, incision is reaching almost the entire catchment leading to a local relief increase (Fig. 5 C-F). Consequently, the highland and escarpment parts are becoming less distinguishable; the differences between them can still be noted since segments above the knickpoint have a subtle lower relief than the ones below. The mean erosion

rate at this stage is closest than those of typical escarpment catchments (Fig. 4).

All the river courses in the escarpment catchment P27 have similar shape. A subtle knickpoint in the main course may record capture (Fig. 9C). At this stage, incision is occurring throughout the catchment and the mean slope angle is approaching the threshold value (Table 2, Fig. 6), indicating that landslides are the dominant erosional process (Montgomery and Brandon, 2002; Ouimet et al., 2009; DiBiase et al., 2010; Scherler et al., 2014). Translational landslides are frequent in Serra do Mar during the high-intensity rainfall events in the summer months (De Ploey and Cruz, 1979). They occur preferentially on hillslope segments where the angle is between 18° and 37° (Fernandes et al., 2004). This range encompasses the mean slope angles of most escarpment and mixed catchments of Serra do Mar and other regions (Table 2). The threshold defined by equation 2 (30°) is close to the average for the mountain range (Fig. 6A). When this stage is reached, a feedback is expected: the relief increase generated by river incision is balanced by landslides in segments of hillslope that reach the threshold angle (Montgomery, 2001), such that the material mobilized by landslides provides abrasive power for river incision (Egholm et al., 2013). Römmer (2008) argued that the continuous balance between river incision and mass movement on hillslopes produces an “upper denudation level” in the Serra do Mar. Consequently, the local relief does not exceed a critical altitude, remaining in a steady state.

Following the episodic capture events, the discontinuous retreat of local escarpments consumes the low relief plateau until it reaches the continental divide. This is best demonstrated in Itatiaia plateau. There seems to be two

distinct escarpment steps in the Itatiaia region (Figure 3E). Rio Preto river flows between these two steps into Paraiba do Sul Valley (Fig. 2B), a consequence of river capture in the Miocene (Rezende et al., 2013). The capture led to the dissection of the Itatiaia plateau and promoted the migration of the escarpment from the first step to the second, the more important regional divide (Figures 2B, C and 3E). The rivers on the other side of the regional divide are also strongly incised and the slope angles approach the threshold value (Fig. 6). This results in relatively high erosion rates for some of the highland catchments in this region (ε > 10 m/Ma, Table 2 and Figure 4) (Salgado et al. 2016). The similarity of erosion rates and topography on both sides of the regional divide suggests that the Itatiaia plateau is losing the classic passive margin morphology and is approaching topographic steady-state (Hack, 1975; Matmon et al., 2003).

5.2. Long-term controls on erosion

A litho-structural control has been invoked to explain escarpment evolution in southeastern Brazil (Almeida and Carneiro, 1998; Romër, 2008) and in passive margins more generally (Gunnel and Harbor, 2010; Scharf et al., 2013). The contrast between litho-types within the catchments leads to differential erosion. This, together with the structural pattern defines weakness lines where incision and captures took place (Gunnel and Harbor, 2010). The lack of relation between erosion rates and lithology in the study area is probably due the gneiss-granite dominance in all analyzed catchments; differences between these two, although may exist (Fig. 7), is masked by stronger controls as climate and topographic relief.

Neotectonic activity may also contribute with river captures and base level change. Based on morphotectonic landforms and tectonic displacement in Pleistocene/Holocene colluvium deposits Modenesi-Gauttierri et al. (2002) have proposed that river capture and base level changes in Campos do Jordão plateau may have been triggered by tectonics. However, the small fault displacement of Pleistocene/Holocene deposits (few cm) and the ubiquity of river capture across the region (Sordi et al. 2018) suggests that tectonics likely has only a limited effect on driving erosion.

This study demonstrates that the prevailing climate has a first-order control on erosion rates across the region (Fig. 8). It is likely that the river incision is governed by precipitation (Fig. 7C) that increases local relief. The high intensity precipitation events trigger landslides in hillslope segments that are close threshold angle (De Ploey and Cruz, 1979). Finally, the availability of water on steep slopes ensures the hydrological conditions for transportation of the mobilized material. However, it is the coupling of high precipitation with high temperature that seems to distinguish the Serra do Mar from other regions. This climatic condition, interacting with a steep relief, results in a landscape with dynamic evolution, where the high erosion rates are likely coupled to fast soil production (Riebe et al., 2003; Heimsath et al., 2006). The high humidity and temperature of Serra do Mar accelerate chemical weathering, which produces friable material of contrasting permeability which favors the occurrence of slope wash and shallow mass movement (Furian et al., 1999; da Silva et al., 2016). Dixon et al. (2009) identified and detailed the relationship between erosion rate-soil production and humidity-temperature in Sierra Nevada.

In the ocean-facing escarpment of Serra do Mar erosion rates are integrated over 11 to 22 ka (except A1) (Table 2). Moisture enough to maintain a variable extent of conifer forest is present in the last 30 ka (Pessenda et al., 2009, Cruz et al., 2009, Pivel et al., 2010) and a discontinuous increase in the current Atlantic Montane forest started 15 ka, following warm and wet conditions (Pessenda et al., 2009). This suggests that the climate has not changed significantly on the time scale over which the erosional history was recorded and the dynamics above described prevail. However, the most slowly eroding inland escarpments of Campos do Jordão, Itatiaia, Bocaina and Quebra-Cangalha are integrated over between 25 and 58 ka (Table 2). The current humidity and temperature, conducive for Montane Atlantic forest, has been attained only in the last 3,000 years (Behling 1997). From the Last Glacial Maximum to the Holocene the climate was colder and dryer than today (Behling, 1997; Behling et al. 2007; Garcia et al., 2004). Under these conditions, erosional pulses (Modenesi-Gautierri, 2000*)* may have been triggered by millennial and orbital climatic oscillations that affected humidity (Cruz et al., 2009). Since the current climate does not have the erosional power of the coastal Serra do Mar, these cyclical erosional pulses define the rates. Colluvium in the highland areas of Campos do Jordão, Itatiaia and Bocaina plateaus record these erosional pulses (Modenesi-Gautierri, 2000; Hiruma et al., 2013). The low relief of the highland regions ensures the long-term preservation of the colluvium, leading to the catchment-scale low erosion rates, within an integration time that reaches 116 ka.

In the long-term, rock uplift is expected to maintain the elevation of the highland regions that sustain the fluvial dissection in the escarpments and to

balance the erosion in the regional divide, thus, maintaining a topographic steady-state. Modenesi-Gautierri et al. (2011) identified changes in pedogenetic processes in Campos do Jordão highlands, which they interpreted as the result of recent adaption to tropical high-altitude climate, reached from ongoing uplift. Post-breakup tectonic reactivation led to rock uplift and landscape rejuvenation during Upper Cretaceous, Paleogene and Miocene (Cobbold et al., 2001; Cogné et al., 2011). The present day erosion rates measured here are significantly lower than the erosion rates estimated during these reactivation phases (up 100 m/Ma; Cogné et al., 2012). Instead, the rates are typical of catchment-averaged erosion rates determined at the most of other stable passive margins, which rarely exceed 100 m/Ma (see Table 2 in Gonzalez et al., 2016). This is consistent with attenuation on tectonic activity after at least the Middle Pleistocene (Salgado et al., 2016) and reinforces the current low stress regime of the continental margin of southeast Brazil (Assumpção, 1998; Gonzalez et al., 2016). Thus, we consider that the landscape evolution has been slow during the Quaternary. A feedback between erosional unloading and isostatically-driven passive uplift becomes an important evolutionary process of the landscape (Bishop and Brown, 1992; Baldwin et al., 2003). If erosion rate is related to rock uplift rates in mountain ranges characterized by hillslopes with threshold angle (Burbank et al., 1996; Montgomery, 2001), it is reasonable that the climatically defined erosion concentrated in the steep escarpments combined with the regional stress is responsible for the highland uplift, which sustains the incision of the rivers in the escarpment.

These findings suggest that the interaction between climate and topographic relief plays a key role in controlling modern day erosion rates in

areas of low tectonic activity. The relevance of this interaction has been underestimated in other studies in passive margins (von Blanckenburg, 2005; Bierman et al., 2014; Mandal et al., 2015). We suggest that the robust correlation between topographic relief and erosion rates has masked the role of climate. A minimum topographic relief is a precondition for triggering erosive processes. Thus, the climatic influence in erosion becomes evident in hillslopes that are close to the threshold angle. von Blanckenburg (2005) reported low erosion rates of the low relief highlands of Sri Lanka and Namibia, around 10 m/Ma (Bierman and Caffee, 2001), noting that they occurred despite the huge difference in precipitation rates. However, in the steep escarpments of Sri Lanka erosion rates approach 70 m/Ma (Vanacker et al., 2007). This differs considerably from similar regions in Namibia, which erode at lower than 20 m/Ma. It is exactly the same in Southeast Brazil, whilst the Serra do Mar escarpment catchments erode twice as fast as the other escarpments, the low relief highland areas erode at similar rates to other highlands catchments in the region (Figure 4). Warm and wet tropical dynamics lead to the weathering mantle thickening and to the erosion rate reduction in the low-relief highland (von Blanckenburg et al. (2004); however, at high-relief such dynamics provides conditions to maintain active erosional processes and the inland migration of the escarpments.

7. Conclusions

We have presented ^{10}Be-derived catchment mean erosion rates for the continental margin of southeastern Brazil. Their relationships with aspects of the topography, climate and geology lead to several conclusions:

1. Low relief highland catchments have the lowest erosion rates in the region (ε = 5–15 m/Ma). The ocean-facing escarpment catchments in Serra do Mar (ε = 18–53 m/Ma) erode twice as fast as those escarpment-dominated catchments inland (ε = 7–24 m/Ma).
2. A balance between river incision and hillslope processes are responsible for maintaining the high relief in the escarpments. Long-term uplift related to regional stress and isostatic response to erosion is expected to strengthen this mechanism.
3. Episodic river captures as recorded in the mixed topography catchments result in the dissection of the highlands and the excavation and migration of escarpments inland. This proceeds discontinuously until it reaches the regional drainage divide.
4. The ocean-facing escarpments of Serra do Mar have the high precipitation and temperature that differentiates them from the other regions. These generate fast chemical weathering and intense river incision and facilitating circumstances to slope wash and shallow mass movement in segments of hillslopes at threshold angle of stability.
5. These climatic conditions have prevailed in the Serra do Mar over much of the time that the cosmogenic ^{10}Be records erosion (~15 ka).
6. Inland, the escarpment areas record a long-term erosion pattern marked cyclical climatic oscillations.

Overall, the results reinforce the need to consider the climatic role in the evolution of a high-altitude passive margin landscapes. Wet and warm tropical climate, as southeaster Brazil, South India, Sri Lanka and others, impose a

specific dynamic, which keeps the escarpment fronts in movement even under relatively low tectonic activity.

Acknowledgements

This research was supported by grant #2014/14702-0 and #2016/10014-7, São Paulo Research Foundation (FAPESP) to PH. DGS was supported by *Coordination for the Improvement of Higher Education Personnel* under Science without Border program (CAPES, 99999.002505/2015-00). FNP was supported by grant #2014/23334-4 from São Paulo Research Foundation (FAPESP). We thank Maria Miguens-Rodriguez and Sheng Xu for their help with the ^{10}Be preparation and measurements, and three journal reviewers for their contributions that have improved this work.

References

Almeida FFM, Carneiro CDR. 1998. Origem e evolução da Serra do Mar. Revista Brasileira de Geociências 28, 135-150.

Assumpção M. 1998. Seismicity and stresses in the Brazilian passive margin. Bulletin of the Seismological Society of America 88, 160–169.

Balco G, Stone JO, Lifton NA, Dunai TJ. 2008. A complete and easily accessible means of calculating surface exposure ages or erosion rates from ^{10}Be and ^{26}Al measurements. Quaternary Geochronology 3, 174–195. DOI: 10.1016/j.quageo.2007.12.001.

Baldwin JA, Whipple KX, Tucker GE. 2003. Implications of the shear stress river incision model for the timescale of postorogenic decay of topography. Journal of Geophysical Research 108, 2158. DOI: 10.1029/2001JB000550

Balestrieri ML, Stuart FM, Persano C, Abbate E, Bigazzi G. 2005. Geomorphic development of the escaprment of the Eritrean margin, southern Red Sea: Combined use of fission track and (U-Th)/He Thermochronometry. Earth and Planetary Science Letters 231, 97-110. DOI: 10.1016/j.epsl.2004.12.011.

Barreto HN, Varajão CAC, Braucher R, Bourlès DL, Salgado AAR, Varajão AFDC. 2013. Denudation rates of the Southern Espinhaço range, Minas Gerais, Brazil, determined by in situ-produced cosmogenic beryllium-10. Geomorphology 191, 1–13. DOI: 10.1016/j.geomorph.2013.01.021.

Behling H. 1997. Late Quaternary vegetation, climate and fire history from the tropical mountain region of Morro de Itapeva, SE Brazil. Palaeogeography, Palaeoclimatology, Palaeoecology 129, 407–422. DOI: 10.1016/S0031-0182(97)88177-1.

Behling, H., Dupont, L., Safford, H. D. & Wefer, G. 2007: Late Quaternary vegetation and climate dynamics in the Serra da Bocaina, southeastern Brazil. Quaternary International 161, 22–31. DOI: 10.1016/j.quaint.2006.10.021.

Bierman PR, Caffee M. 2001. Slow rates of rock surface erosion and sediment production across the Namib Desert and escarpment, southern Africa. American Journal of Science 301, 326–358. DOI: 10.2475/ajs.301.4-5.326.

Bierman PR, Coppersmith R, Hanson K, Neveling J, Portenga EW, Rood DH. 2014. A cosmogenic view of erosion, relief generation, and the age of faulting in southern Africa. GSA Today 24, 4–11. DOI: 10.1130/GSATG206A.1.

Bishop P, Brown R. 1992. Denudational isostatic rebound of intraplate highlands: The Lachlan River valley, Australia, Earth Surface Processes and Landforms 17, 345-360.

Bookhagen B, Strecker MR. 2012. Spatiotemporal trends in erosion rates across a pronounced rainfall gradient: Examples from the southern Central

Andes. Earth and Planetary Science Letters 327-328, 97–110. DOI: 10.1016/j.epsl.2012.02.005.

Braun J, Simon-Labric T, Murray KE, Reiners PW. 2014. Topographic relief driven by variations in surface rock density. Nature Geoscience 7, 534–540. DOI: 10.1038/ngeo2171.

Burbank DW, Leland J, Fielding E, Anderson RS, Brozovic N, Reid MR, Duncan C. 1996. Bedrock incision, rock uplift and threshold hillslopes in the northwestern Himalayas. Nature 379, 505–510. DOI: 10.1038/379505a0.

Cherem LFS, Varajão CAC, Braucher R, Bourlés D, Salgado AAR, Varajão AC. 2012. Long-term evolution of denudational escarpments in southeastern Brazil. Geomorphology 173-174, 118–127. DOI: 10.1016/j.geomorph.2012.06.002.

Cobbold PR, Meisling KE, Mount VS. 2001. Reactivation of na obliquely rifted margin, Campos and Santos Basins, southeastern Brazil. AAPG Bulletin 85, 1925–1944. DOI: 10.1306/8626D0B3-173B-11D7-8645000102C1865D.

Cogné N, Gallagher K, Cobbold PR. 2011. Post-rift reactivation of the onshore margin of southeast Brazil: evidence from apatite (U–Th)/He and fission-track data. Earth and Planetary Science Letters 309, 118–130. DOI:10.1016/j.epsl.2011.06.025.

Cogné N, Gallagher K, Cobbold PR, Riccomini C, Gautheron C. 2012. Post-breakup tectonics in southeast Brazil from thermochronological data and combined inverse-forward thermal history modeling. Journal of Geophysical Research 117, B11413. DOI:10.1029/201 2JB009340.

Codilean, A.T. 2006. Calculation of the cosmogenic nuclide production topographic shielding scaling factor for large areas using DEMs. Earth Surface Processes and Landforms 31, 785–794. DOI: 10.1002/esp.1336.

Cruz FW, Wang X, Auler A, Vuille M, Burns SJ, Edwards LR, Karmann I, Cheng H. 2009. Orbital and millennial-scale precipitation changes in Brazil from speleothem records. In Past Climate Variability in South America and Surrounding 29 Regions: From the Last Glacial Maximum to the Holocene, Vimeux F, Sylvestre F, Khodri M (eds). Springer, Dordrecht, The Netherlands, 29–60.

da Silva AS, Guerra AJT, Polivanov H, Fullen MA. 2016. Soil structural indicators of hillslope destabilization in the Serra do Mar mountain range (Rio de Janeiro State, Brazil). Natural Hazards 81, 1177. DOI:10.1007/s11069-015-2126-7

de Ploey J, Cruz O.1979. Landslides in the Serra do Mar, Brazil. Catena 6, 111–122. DOI: 10.1016/0341-8162(79)90001-8.

DiBiase RA, Whipple KX, Heimsath AM, Ouimet WB. 2010. Landscape form and millennial erosion rates in the San Gabriel Mountains, CA. Earth and Planetary Science Letters 289, 134–144. DOI: 10.1016/j.epsl.2009.10.036.

Dixon JL, Heimsath AM, Amundson R. 2009. The critical role of climate and saprolite weathering in landscape evolution. Earth Surface Process and Landforms 34, 1507–1521. DOI: 10.1002/esp.1836.

Egholm, DL, Knudsen, MF, Sandiford, M. 2013. Lifespan of mountain ranges scaled by feedbacks between landsliding and erosion by rivers. Nature 498, 475–478. DOI: 10.1038/nature12218.

Farr TG, Rosen PA, Caro E, Crippen R, Duren R, Hensley S, Kobrick M, Paller M, Rodriguez E, Roth L, Seal D, Shaffer S, Shimada J. Umland J. 2007, The Shuttle Radar Topography Mission. Review of Geophysics 45, 1-34. RG2004. DOI:10.1029/2005RG000183.

Fernandes NF, Guimarâres RF, Gomez RAT, Vieira BC, Montgomery DR, Greenberg H. 2004. Topographic controls of landslides in Rio de Janeiro: field

evidence and modeling. Catena 55, 163–181. DOI: 10.1016/S0341-8162(03)00115-2.

Fick S, Hijmans R. 2017. WorldClim 2: New 1-km spatial resolution climate surfaces for global land areas. International Journal of Climatology. DOI: 10.1002/joc.5086.

Flint JJ. 1974. Stream gradient as a function of order, magnitude, and discharge. Water Resources Research 10, 969–973. DOI: 10.1029/WR010i005p00969.

Furian S, Barbiéro L, Boulet R. 1999. Organisation of the soil mantle in tropical southeastern Brazil (Serra do Mar) in relation to landslides processes. Catena 38, 65–83. DOI: 10.1016/S0341-8162(99)00015-6.

Gallagher K, Hawkesworth CJ, Mantovani MSM. 1994. Denudation, fission track analysis and the long-term evolution of passive margin topography: application to the southeast Brazilian margin. Journal of South American Earth Sciences 8 (1), 65–77. DOI: 10.1016/0895-9811(94)00042-Z.

Garcia MJ, Oliveira PE, Siqueira E, Fernandes RS. 2004. A Holocene vegetational and climatic record from the Atlantic rainforest belt of coastal State of São Paulo, SE Brazil. Review of Palaeobotany and Palynology 131, 181-199. DOI: 10.1016/j.revpalbo.2004.03.007.

Gonzalez VS, Bierman PR, Fernandes NF. 2016. Long-term background denudation rates of southern and southeastern Brazilian watersheds estimated with cosmogenic ^{10}Be. Geomorphology 268, 54–63. DOI: 10.1016/j.geomorph. 2016.05.024.

Gunnell Y, Harbor D. 2010. Butte detachment: how pre-rift geological structure and drainage integration drive escarpment evolution at rifted continental margins. Earth Surface Processes and Landforms 35, 1373–1385. DOI: 10.1002/ esp.1973.

Hack JT. 1975. Dynamic equilibrium and landscape evolution. In Theories of landform development, Melhorn WN, FLEMAL RC (eds). Allen & Unwin: London pp 87-102.

Hackspacher PC, Ribeiro LFB, Ribeiro MCS, Fetter AH, Hadler Neto JC, Tello Saenz CA, Dantas EL. 2004. Consolidation and break-up of the South American platform in SE Brazil: tectonothermal and denudation Histories. Gondwana Research 7, 91–101. DOI: 10.1016/S1342-937X(05)70308-7.

Heilbron M, Pedrosa-Soares AC, Campos Neto MC, Silva LC, Trouw RAJ, JanasI VA. 2004. Província Mantiqueira, p. 204-234. In Geologia do Continente Sul-Americano: Evolução da Obra de Fernando Flávio Marques de Almeida, Mantesso-Neto V, Bartorelli A, Carneiro CDR, Brito-Neves BB. (eds), Beca: São Paulo 647p.

Heilbron M, Almeida JCH, Eirado LG, Palermo N, Tupinambá M, Duarte BP, Valladares C, Ramos R, Sanson M, Guedes E, Gontijo A, Nogueira JR, Valeriano C, Ribeiro A, Ragatky CD, Miranda A, Sanches L, Melo CL, Roig HL, Dios FB, Fernández G, Neves A, Guimarães P, Dourado F, Lacerda VG. (Org) 2007. Volta Redonda- SF.23-Z-A-V, escala 1:100,000: nota explicativa integrada com Santa Rita do Jacutinga, Barra do Piraí, Angra dos Reis. Rio de Janeiro/São Paulo: UERJ/CPRM.

Heilbron M, Eirado LG, Almeida J. (Org) 2016. Geologia e recursos minerais do Estado do Rio de Janeiro: texto explicativo do mapa geológico e de recursos minerais, escala 1:400,000. Belo Horizonte, CPRM.

Heimsath AM, Chappel J, Finkel RC, Fifield K, Alimanovic A. 2006. Escarpment erosion and landscape evolution in southeastern Australia. In Tectonics, Climate, and Landscape Evolution: Geological Society of America, Willett SD, Hovius N, Brandon MT, Fisher DM (eds), Special Paper 398, 173–190.

Heimsath AM, Fink D, Hancock GR. 2009. The 'humped' soil production function: eroding Arnhem Land, Australia. Earth Surface Processes and Landforms 34 (12), 1674–1684. DOI: 10.1002/esp.1859.

Hijmans RJ, Cameron SE, Parra JL, Jones PG, Jarvis A. 2005. Very high resolution interpolated climate surfaces for global land areas. International Journal of Climatology 25 (15), 1965–1978. DOI: 10.1002/joc.1276.

Hiruma ST, Riccomini C, Modenesi-Gautierri MC, Hackspacher PC, Hadler Neto JC, Franco-Magalhães AOB. 2010. Denudation history of the Bocaina Plateau, Serra do Mar, southeastern Brazil: Relationships to Gondwana breakup and passive margin development. Gondwana Research 18, 674–687. DOI: 10.1016/j.gr.2010.03.001.

Hiruma ST, Modenesi-Gauttieri MC, Riccomini C. 2012. Late Quaternary colluvial deposits in the Bocaina Plateau, southeastern Brazil highlands: age and palaeoenvironmental consequences. Boreas 42, 306-316. DOI: 10.1111/j.1502-3885.2012.00272.x.

Leite YLR, *Costa LP,* Loss AC, Rocha RG., Batalha-Filho H, Bastos *AC, Q*uaresma VS, Fagundes V, Paresque R, Passamani M, Pardini *R.* 2016. Neotropical forest expansion during the last glacial period challenges refuge hypothesis. Proceedings of National Academy of Sciences 113, 1008–1013. DOI: 10.1073/pnas.1513062113.

Mandal SK, Lupker M, Burg J, Valla PG, Haghipour N, Christl M. 2015. Spatial variability of ^{10}Be-derived erosion rates across the southern Peninsular Indian escarpment: A key to landscape evolution across passive margins. Earth and Planetary Science Letters 425, 154–167. DOI: 10.1016/j.epsl.2015.05.050.

Matmon A, Bierman P, Enzel Y. 2002. Pattern and tempo of great escarpment erosion. Geology ; 30 (12): 1135–1138. DOI: 10.1130/0091-7613(2002)030<1135:PATOGE>2.0.CO;2

Matmon A, Bierman PR, Larsen J, Southworth S, Pavich M, Finkel R, Caffee M. 2003. Erosion of an ancient mountain range, the Great Smokey Mountains, North Carolina and Tennessee. American Journal of Science 303, 817–855. DOI: 10.1016/j.epsl.2015.05.050.

Modenesi-Gauttieri, MC. 2000: Hillslope deposits and the Quaternary evolution of the altos campos – Serra da Mantiqueira, from Campos do Jordão to the Itatiaia Massif. Revista Brasileira de Geociências 30, 508–514.

Modenesi-Gauttieri MC, Hiruma ST, Riccomini C. 2002. Morphotectonics of a high plateau on the northwest flank of the continental rift of Southeastern Brazil. Geomorphology 43, 257-271. DOI: 10.1016/S0169-555X(01)00137-4.

Modenesi-Gauttieri MC, de Toledo MCM, Hiruma ST, Taioli F, Shimada H. 2011. Deep weathering and landscape evolution in a tropical plateau. Catena 85, 221–230, DOI:10.1016/j.catena.2011.01.006.

Montgomery DR. 2001. Slope distributions, threshold hillslopes, and steady-state topography. American Journal of Science 301, 432-454. DOI: 10.2475/ajs.301.4-5.432.

Montgomery DR, Brandon MT. 2002. Topographic controls on erosion rates in tectonically active mountain ranges. Earth and Planetary Science Letters 201, 481–489. DOI: 10.1016/S0012-821X(02)00725-2.

Morais, SM. (Org) 1999. Programa Levantamentos Geológicos Básicos do Brasil: Integração geológica da folha Santos SF.23-Y-D: escala 1:250.000: estado de São Paulo: nota explicativa. São Paulo: CPRM.

Nichols KK, Bierman P, Rood DH. 2014. ^{10}Be constrains the sediment sources and sediment yields to the Great Barrier Reef from the tropical Barron River catchment, Queensland, Australia. Geomorphology 224, 102–110. DOI: 10.1016/j.geomorph.2014.07.019.

Ouimet WB, Whipple KX, Granger DE. 2009. Beyond threshold hillslopes: channel adjustment to base-level fall in tectonically active mountain ranges. Geology 37, 579–582. DOI: 10.1130/G30013A.1.

Pedrosa Soares AC, Noce CM, Trouw RAJ, Heilbron M. (Org.). 2003. Geologia e Recursos Minerais do Sudeste Mineiro, Projeto Sul de Minas- Etapa I. Belo Horizonte: COMIG- Companhia Mineradora de Minas Gerais. CD-ROM.

Persano C, Stuart FM, Bishop P, Barfod DN. 2002. Apatite (U-Th)/He age constraints on the development of the Great Escarpment of the southeastern Australian passive margin. Earth and Planetary Science Letters 200, 79–90. DOI: 10.1016/S0012-821X(02)00614-3.

Pessenda LCR, Oliveira PE, Mofatto M, Medeiros VB, Garcia RJF, Aravena R, Bendassoli JÁ, Leite AZ, Saad AR, Etchebehere ML. 2009. The evolution of a tropical rainforest/grassland mosaic in southeastern Brazil since 28,000 ^{14}C yr BP based on carbon isotopes and pollen records. Quaternary Research 71, 437–452. DOI: 10.1016/j.yqres.2009.01.008.

Perrota MM, Salvador ED, Lopes RC, D'Agostinho, LZ. (Org), 2005. Mapa geológico do estado de São Paulo, escala 1:750.000. Programa levantamentos geológicos básicos do Brasil, São Paulo: CPRM.

Peternel R, Trouw R, Vinagre R, Fontainha M, Correa R, Reis R, Meireles M, Lages M. (Org). 2014. Carta geológica: folha Campos do Jordão, SF. 23-YBV. Rio de Janeiro/São Paulo: UERJ/CPRM.

Pivel MAG, Toledo FAL, Costa KB. 2010. Foraminiferal record of changes in summer monsoon precipitation at the southeastern Brazilian continental margin since the Last Glacial Maximum. Revista Brasileira de Paleontologia 13, 79–88. DOI: 10.4072/rbp.2010.2.01.

Portenga EW, Bierman PR. 2011. Understanding Earth's eroding surface with ^{10}Be. Geological Society of America Today 21, 4–10. DOI: 10.1130/G111A.1.

Pupim FN, Bierman PR, Assine ML, Rood DH, Silva A, Merino ER. 2015. Erosion rates and landscape evolution of the lowlands of the Upper Paraguay river basin (Brazil) from cosmogenic ^{10}Be. Geomorphology 234, 151–160. DOI: 10.1016/j.geomorph.2015.01.016.

Radam Brasil. 1983. Secretraria Geral – Ministério de Minas e Energia. Projeto Radam Brasil; Folhas SF 23/24, Rio de Janeiro/Vitória: 32.

Rezende EA, Salgado AAR, da Silva JR, Bourlés D, Leánni L. 2013. Fatores controladores da evolução do relevo no flanco NNW do rift continental do sudeste do Brasil: Uma análise baseada na mensuração dos processos denudacionais de longo termo. Revista Brasileira de Geomorfologia 14(2), 221–234. DOI: 10.20502/rbg.v14i2.416.

Riccomini C, Assumpção M. 1999. Quaternary tectonics in Brazil. Episodes, 22(3), 221-225. 10.18814/epiiugs/1999/v22i3/62780.

Riccomini C, Sant´Anna LG, Ferrari AL. 2004. Evolução geológica do Rift Continental do Sudeste do Brasil. In Geologia do Continente Sul-Americano: Evolução da Obra de Fernando Flávio Marques de Almeida, Mantesso-Neto V, Bartorelli A, Carneiro CDR, Brito-Neves BB. (eds), Beca: São Paulo 647p.

Riebe CS, Kirchner JW, Finkel RC. 2003. Long-term rates of chemical weathering and physical erosion from cosmogenic nuclides and geochemical mass balance. Geochimica et Cosmochimica Acta 67: 4411–4427. DOI: 10.1016/S0016-7037(03)00382-X.

Roering JJ, Kirchner JW, Dietrich WE. 1999. Evidence for nonlinear, diffusive sediment transport on hillslopes and implications for landscape morphology. Water Resources Research 35, 853–870. DOI: 10.1029/1998WR900090.

Römmer W. 2008. Accordant summit heights, summit levels and the origin of the “upper denudation level” in the Serra do Mar (SE-Brazil, São Paulo): A

study of hillslope forms and processes. Geomorphology 100, 312–327. DOI: 10.1016/j.geomorph.2008.01.001.

Salgado AAR, Braucher R, Varajão AC, Colin F, Varajão AFDC, Nalini JHA. 2008. Relief evolution of the Quadrilátero Ferrífero (Minas Gerais, Brazil) by means of ^{10}Be cosmogenic nuclei. Zeitschrift für Geomorphologie. 52 (3), 317–323. DOI: 10.1127/0372-8854/2008/0052-0317.

Salgado AAR, Marent BR, Cherem LFS, Bourlès D, Santos LJC, Braucher R, Barreto HN. 2014. Denudation and retreat of the Serra do Mar escarpment in southern Brazil derived from in situ-produced 10Be concentration in river sediment. Earth Surface Processes and Landforms, 39, 311–319. DOI: 10.1002/esp.3448.

Salgado AAR, Rezende EA, Bourlès D, Braucher R, da Silva JR, Garcia RA. 2016. Relief evolution of the Continental Rift of Southeast Brazil revealed by in situ-produced ^{10}Be concentrations in river-borne sediments. Journal of South American Earth Sciences 67, 89-99. DOI: 10.1016/j.jsames.2016.02.002.

Sant'Anna Neto J. 2005. Decálogo da climatologia do sudeste brasileiro. 886. Revista Brasileira de Climatologia 1, 43–60. DOI: 10.5380/abclima.v1i1.25232.

Scharf TE, Codilean AT, de Wit M, Jansen JD, Kubik PW. 2013. Strong rocks sustain ancient postorogenic topography in southern Africa. Geology 41, 331–334. DOI: 10.1130/G33806.1.

Scherler D, Bookhagen B, Strecker MR. 2014. Tectonic control on ^{10}Be-derived erosion rates in the Garhwal Himalaya, India. J. Geophys. Res. 119, 83–105. DOI: 10.1002/2013JF002955.

Schwanghart W, Scherler D. 2014. TopoToolbox 2–MATLAB-based software for topographic analysis and modeling in Earth surface sciences. Earth Surface Dynamics 2, 1-7. DOI: 10.5194/esurf-2-1-2014.

Sordi MC, Salgado AAR, Siame L, Bourlès D, Paisani JC, Léanni L, Braucher R, Couto EV, ASTER Team. 2018. Implications of drainage rearrangement for passive margin escarpment evolution in southern Brazil. Geomorphology 306, 155–169. DOI: 10.1016/j.geomorph.2018.01.007.

Stone JO. 2000. Air pressure and cosmogenic isotope production. Journal of Geophysical Research 105, 23753–23759. DOI: 10.1029/2000JB900181.

Sullivan CL. 2007. ^{10}Be erosion rates and landscape evolution of the Blue Ridge escarpment, Southern Appalachian mountains. University of Vermont, Burlington, VT, M.Sc. (76 pp).

Summerfield MA. 1991. Global Geomorphology. Longman Scientific and Technical. Co-published by John Wiley and Sons Inc., New York, 537 pp.

Thomaz Filho A, Cesero P, Mizusaki AM, Leão JG. 2005. Hot spot volcanic tracks and their implications for South American plate motion, Campos basin (Rio de Janeiro state), Brazil. Journal of South American Earth Sciences 18, 383-389. DOI: 10.1016/j.jsames.2004.11.006.

Trouw RAJ, Peternel R, Castro EMO, Trouw CC, Matos GC. 2007. Varginha-SF.23-V-D-VI, escala 1:100.000: nota explicativa integrada com a Folha Itajubá./. - Minas Gerais: CPRM.

Trouw RAJ, Peternel R, Vinagre R, Trouw C, Matos G, Duffles P, Fontainha M. 2014. Carta geológica: folha Pindamonhangaba-SF. 23-YB-VI. Rio de Janeiro/São Paulo: UERJ/CPRM.

Tucker, GE, Slingerland, RL. 1994. Erosional dynamics, flexural isostasy, and long-lived escarpments: A numerical modeling study. Journal of Geophysical Research: Solid Earth, 99(B6), 12229-12243. DOI: 10.1029/94JB00320.

Vanacker V, von Blanckenburg F, Hewaeasam T, 2007. Constraining landscape development of the Sri Lankan Escarpment with cosmogenic nuclides in river

sediment. Earth and Planetary Science Letters 253, 402–414. DOI: 10.1016/j.epsl.2006.11.003.

von Blanckenburg F, Hewawasam T, Kubik PW. 2004. Cosmogenic nuclide evidence for low weathering and denudation in the wet, tropical highlands of Sri Lanka. J. Geophys. Res. 109 (F3). DOI: 10.1029/2003JF000049.

von Blanckenburg F. 2005. The control mechanisms of erosion and weathering at basin scale from cosmogenic nuclides in river sediment. Earth Planetary Science. Letters. 237, 462–479. DOI:10.1016/j.epsl.2005.06.030.

Xu C, Dougans AB, Freeman SPHT, Schnabel C, Wilcken KM. 2010. Improved ^{10}Be and ^{26}Al-AMS with a 5 MV spectrometer. Nuclear Instruments & Methods in Physics Research B 268, 736–738. DOI: 10.1016/j.nimb.2009.10.018.

Whipple, KX. 2004. Bedrock rivers and the geomorphology of active orogens. Annual Review of Earth an Planetary Sciences.32, 151–185. DOI: 10.1146/annurev.earth.32.101802.120356

Wobus C, Whipple KX, Kirby E, Snyder N, Johnson J, Spyropolou K, Crosby B., Sheehan D. 2006. Tectonics from topography: procedures, promise, and pitfalls. Geological Society of America Special Pappers. 398, 55–74. DOI: 10.1130/2006.2398(04).

Zalán PV. 2004. A Evolução Fanerozóica das Bacias Sedimentares Brasileiras. In Geologia do Continente Sul-Americano: Evolução da Obra de Fernando Flávio Marques de Almeida, Mantesso-Neto V, Bartorelli A, Carneiro CDR, Brito-Neves BB. (eds), Beca: São Paulo 647p.

Zalán PV, Oliveira JBA. 2005. Origem e Evolução Estrutural do Sistema de Riftes Cenozóicos do Sudeste do Brasil. Geociências. Petrobras, Rio de Janeiro, 13, 269-300.

Figure Captions

Figure 1. (A) Topographic map of the Atlantic Ocean coast of Brazil. The Serra da Mantiqueira is located to northwest of the Paraíba do Sul River. It is divided into two geomorphological regions: Campos do Jordão plateau (CJ) and Itatiaia plateau (Ita). The Serra do Mar is located to southeast of the Paraíba do Sul river and it is divided into three geomorphological regions: Serra do Mar (SM); Bocaina plateau (Boc); Serra do Quebra Cangalha (SQC). Profiles A-A', B-B' and C-C' are shown in Figure 2. (B) Simplified regional geologic map. The Poços de Caldas–Cabo Frio Alignment is the suite of alkaline bodies along WNW-ESE lineation: Poços de Caldas massif (PCM); Passa Quatro Massif (PQM) and Itatiaia Massif (IM). The Cenozoic Sedimentary Basins: São Paulo basin (SPB), Taubaté basin (TB) and Rezende basin (RB). The states: São Paulo (SP); Minas Gerais (MG) and Rio de Janeiro (RJ). (C) Is the location of the study area.

Figure 2. Topographical profiles identified in Figure 1. Profile A-A' is from the Campos do Jordão plateau to the Serra do Mar. The Sapucaí River is incised in an old shear zone. The Quebra-Cangalha are a mountain belt at the boundary of Serra do Mar and Paraíba do Sul Valley. Profile B-B' is from the Itatiaia plateau to the Bocaina plateau. In the Itatiaia plateau the rivers are strongly incised. Profile C-C' is from the Campos do Jordão plateau to the Itatiaia plateau.

Figure 3. Delineation of the river catchments in this study; (A) Serra do Mar, (B) Serra do Quebra-Gangalha, (C) Bocaina plateau, (D) Campos do Jordão plateau and (E) Itatiaia plateau. Arrows points to the escarpment. Cosmogenic ^{10}Be concentrations from catchments A-E are from Salgado et al. (2016).

Figure 4. Regional distribution of erosion rates plotted according to the catchment type (Highland, Escarpment and Mixed Topography).

Figure 5. Inter-relationship between morphometric parameters. (A) shows the correlation between slope angle and channel steepness index (k_{sn}); (B) shows how local relief (LR) is correlated with slope angle, k_{sn} and erosion rates at all scales. The coefficient correlation (R^2) was estimated by least-squares linear regression. R^2 is plotted according to the LR window radii. CR refers to total catchment relief. (C-F) shows local relief distribution according to catchment type at different windows radii. The colored symbols in (A, C-F) represent catchment types: Highland (H); Escarpment (E) and Mixed (M).

Figure 6. Relationships between cosmogenic ^{10}Be-derived erosion rates and morphometric parameters: (A) Average slope angle shows correlation with model (2); (B) Normalized channel steepness index (k_{sn}) measured with drainage area, and with discharge (C). Both show correlation with model (3). See text for details of models.

Figure 7. Cosmogenic ^{10}Be-derived erosion rates related to litho-types. Arrows indicates the proportion of specific litho-types in catchments of mixed lithology;

granite (grt) and gneiss (gn). * indicates a small content in quartzite. The data symbols are similar to those in Figure 6.

Figure 8. Correlations between cosmogenic ^{10}Be-derived erosion rates and climatic parameters: (A) mean annual precipitation (MAP); (B) mean annual temperature (MAT); and (C) erosion rates determined by a regression model derived from the multiple regression between erosion rates, MAP and MAT. The data symbols are those from Figures 6.

Figure 9. Longitudinal river profiles and slope-area log-log plot of catchments at different evolutionary stage. (A) P24 catchment, Campos do Jordão plateau; (B) P30 catchment, Serra do Mar; and (C) P27 catchment – Serra do Mar. Arrows indicate knickpoints in the longitudinal profiles and their location for each channel in the slope-area plots. The slope-area plots are in the same scale in A, B and C, thus, the scatter can be compared. Locations of the catchments are in Figure 3.

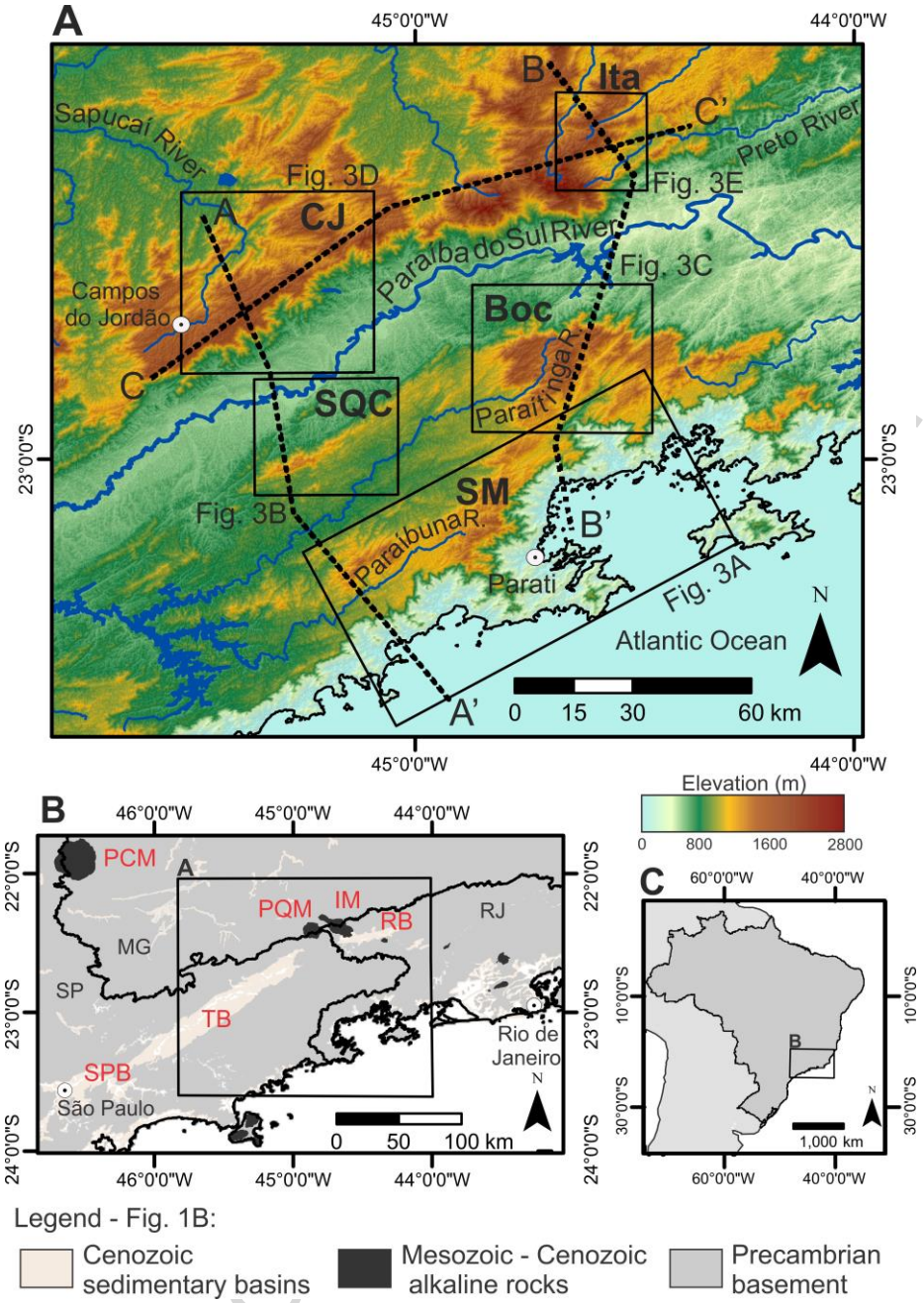

Figure 1

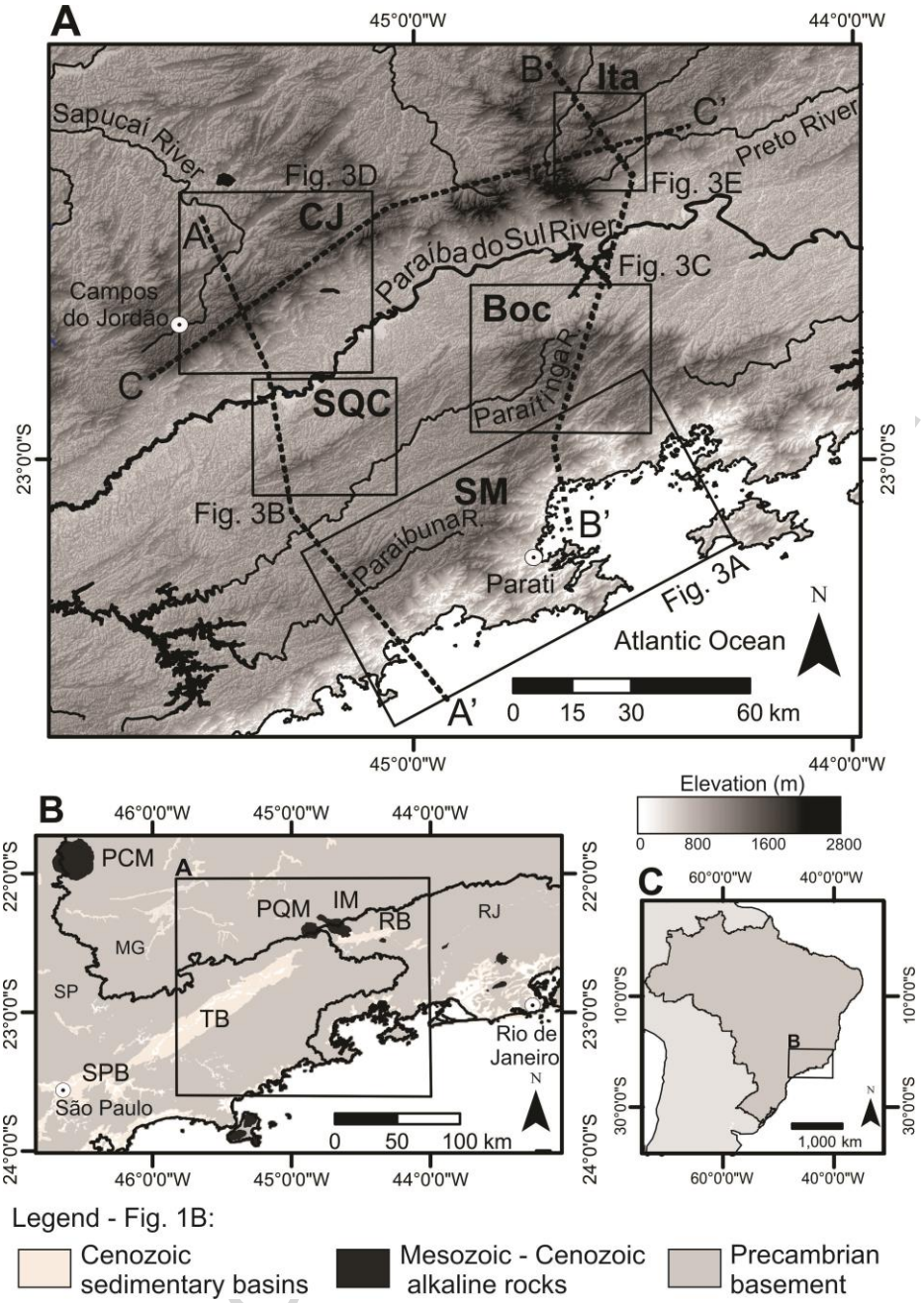

Legend - Fig. 1B:

Cenozoic sedimentary basins

Mesozoic - Cenozoic alkaline rocks

Precambrian basement

Figure 1 (grey scale version)

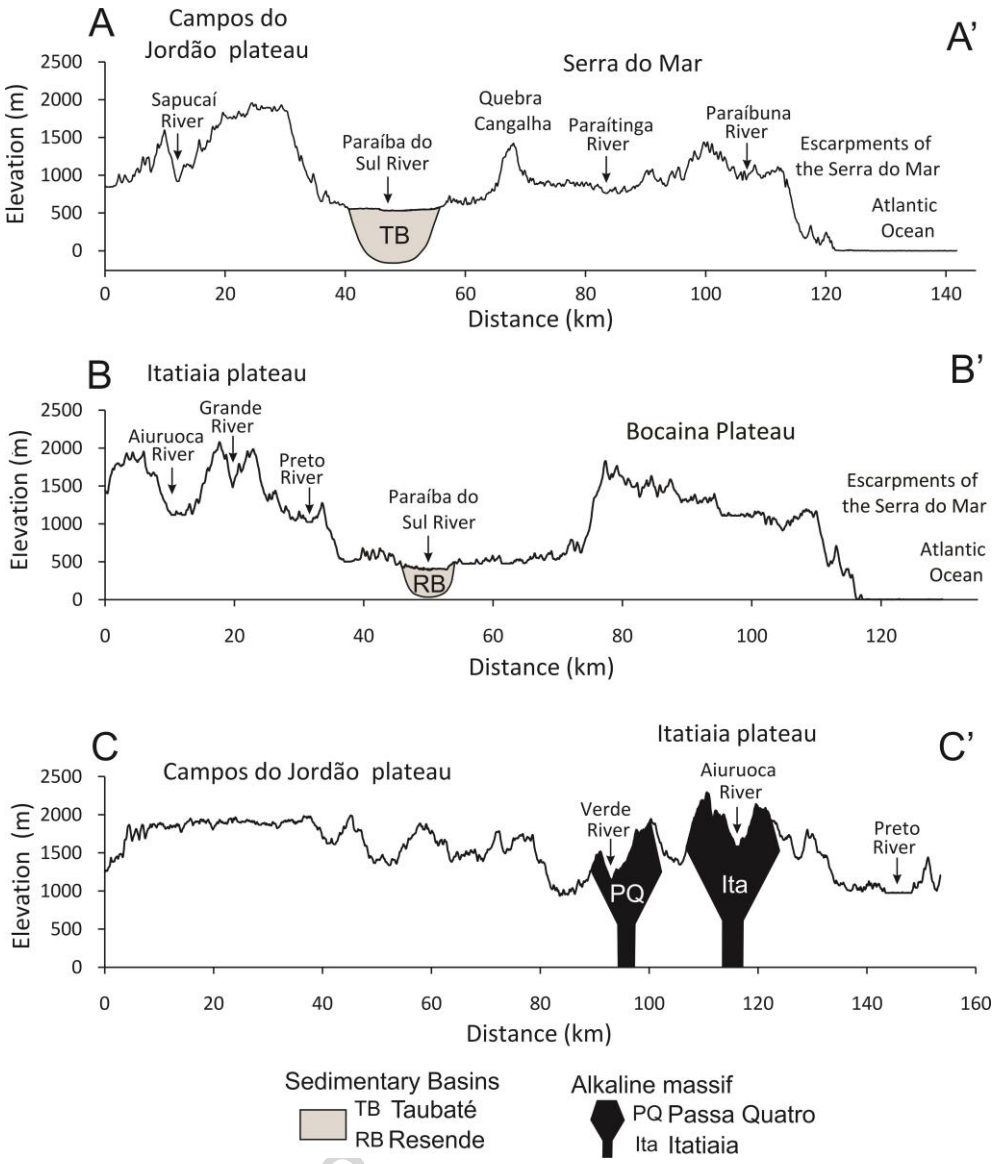

Figure 2

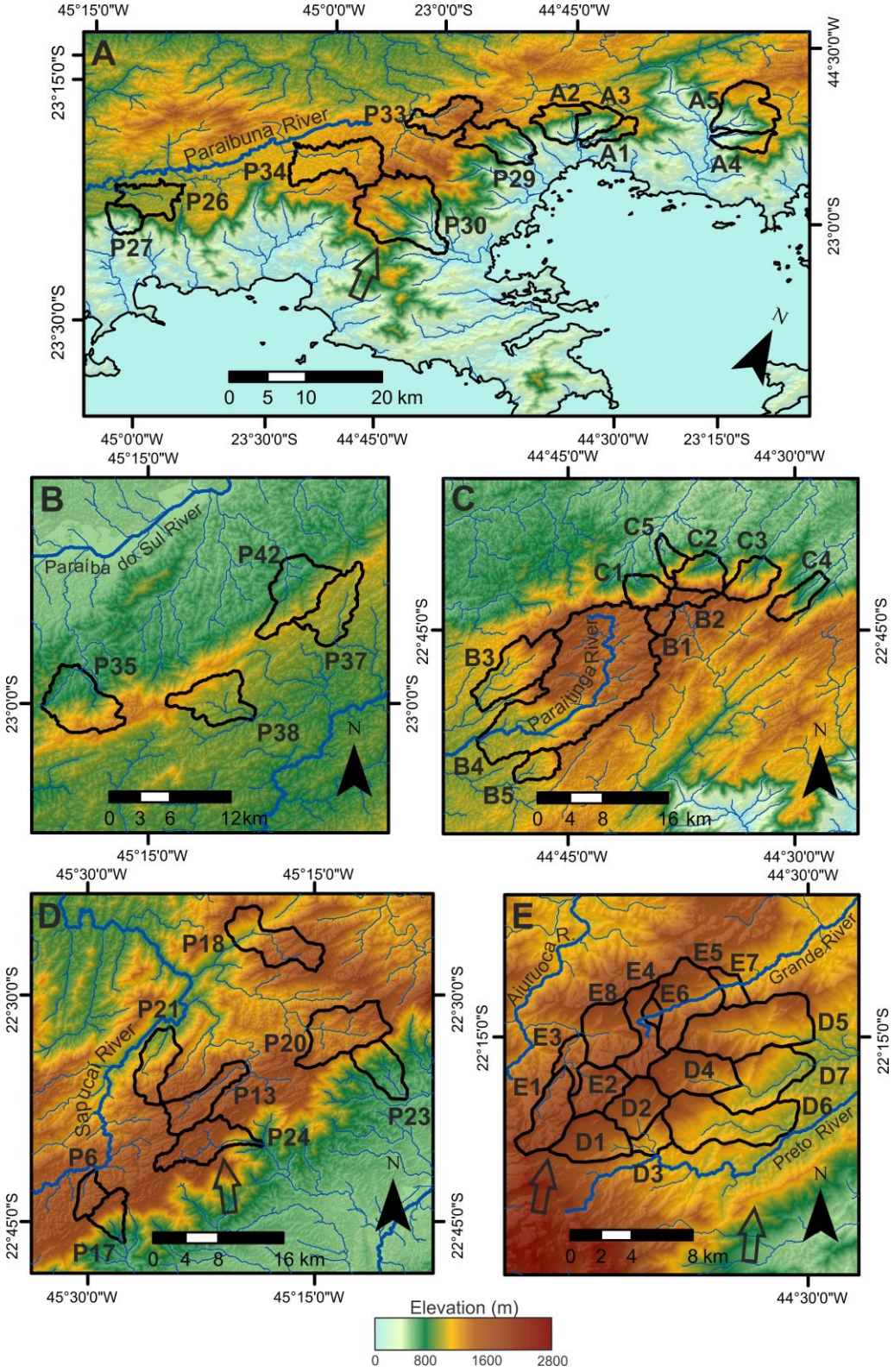

Figure 3

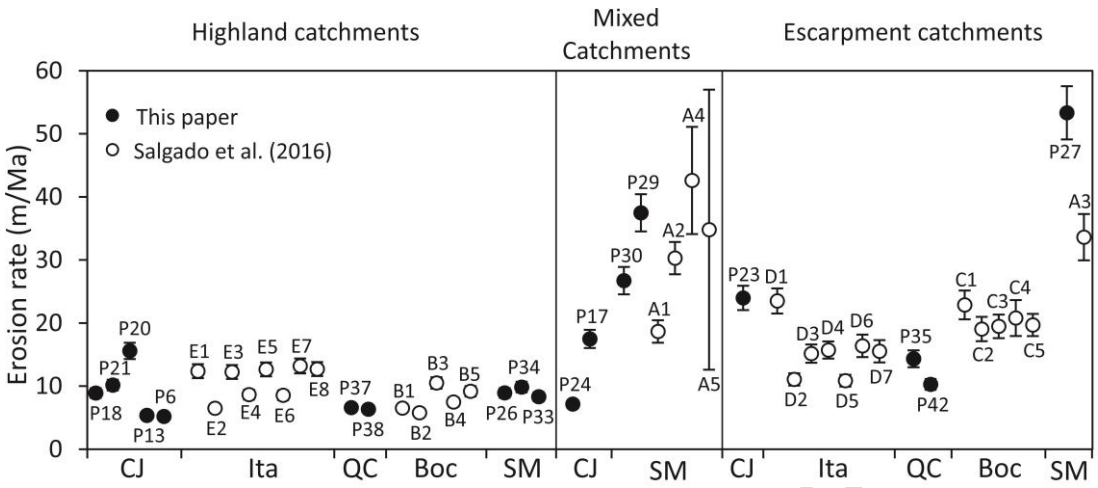

Figure 4

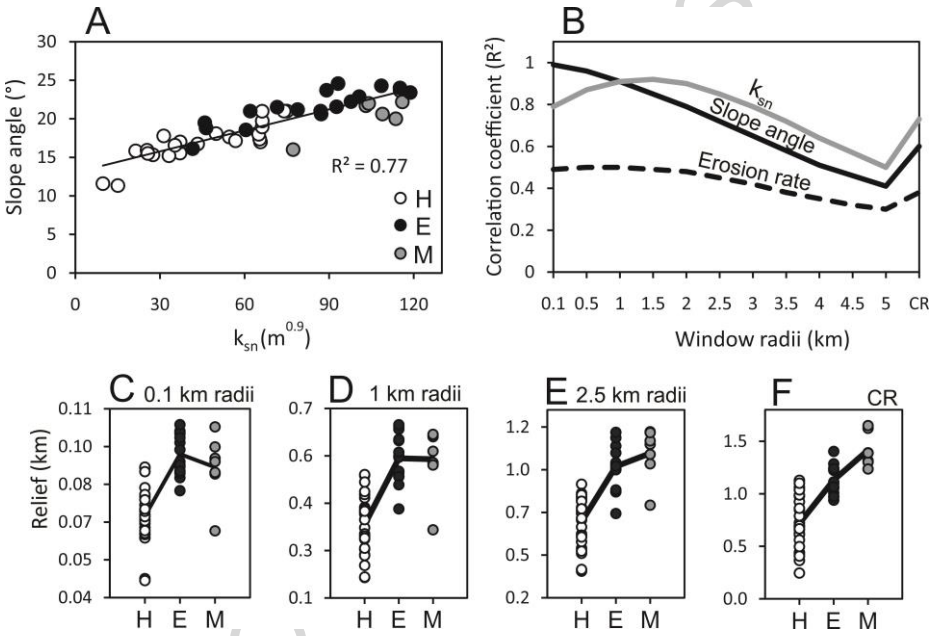

Figure 5

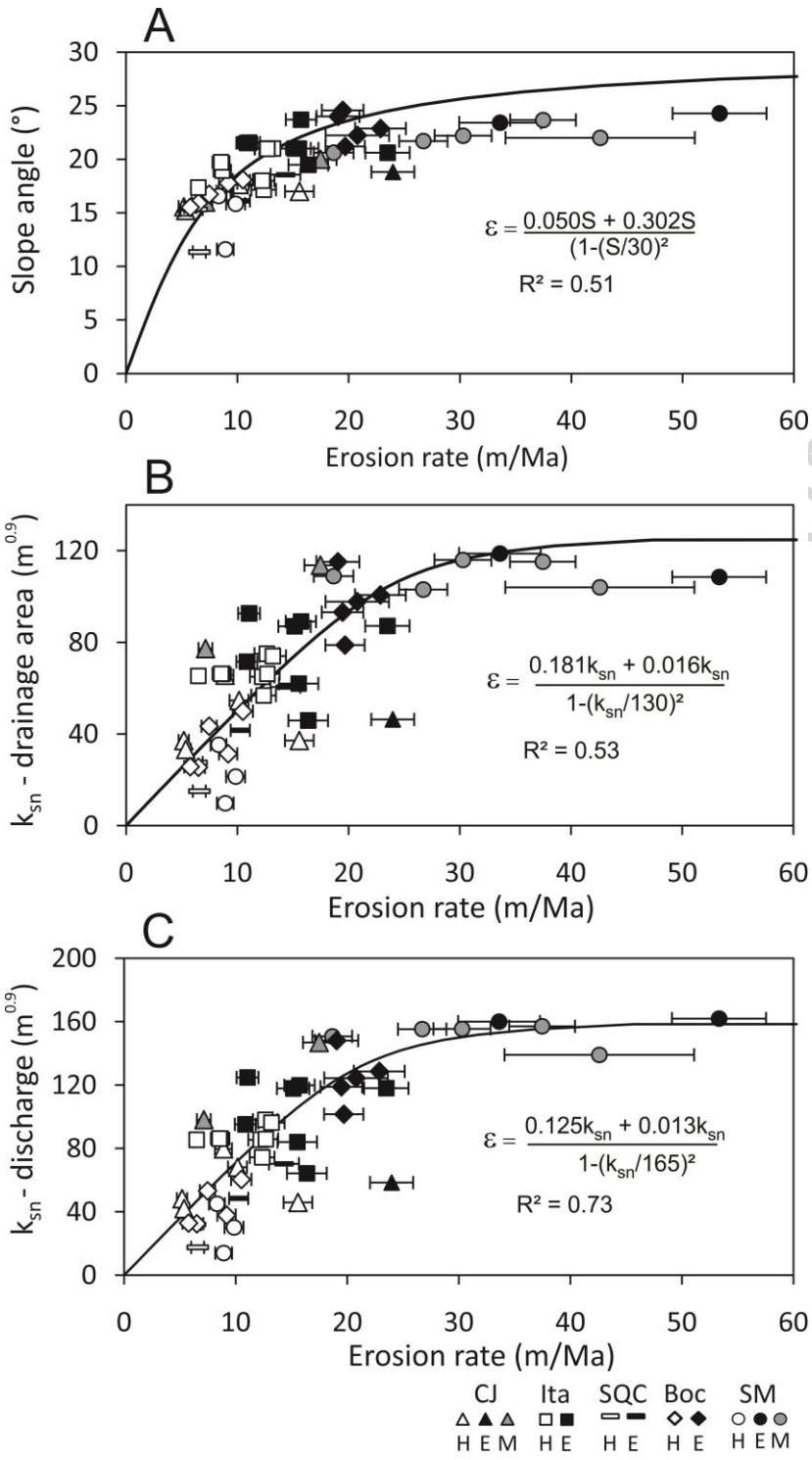

Figure 6

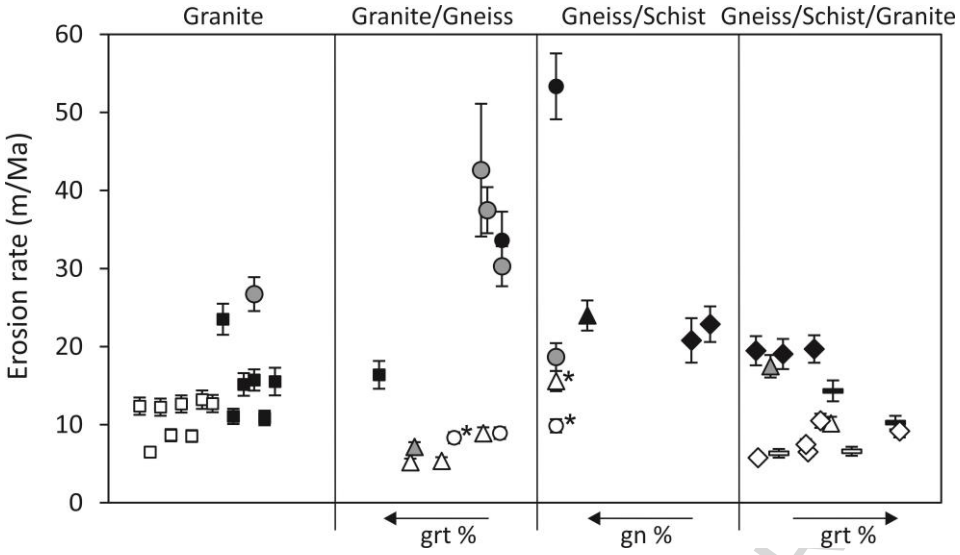

Figure 7

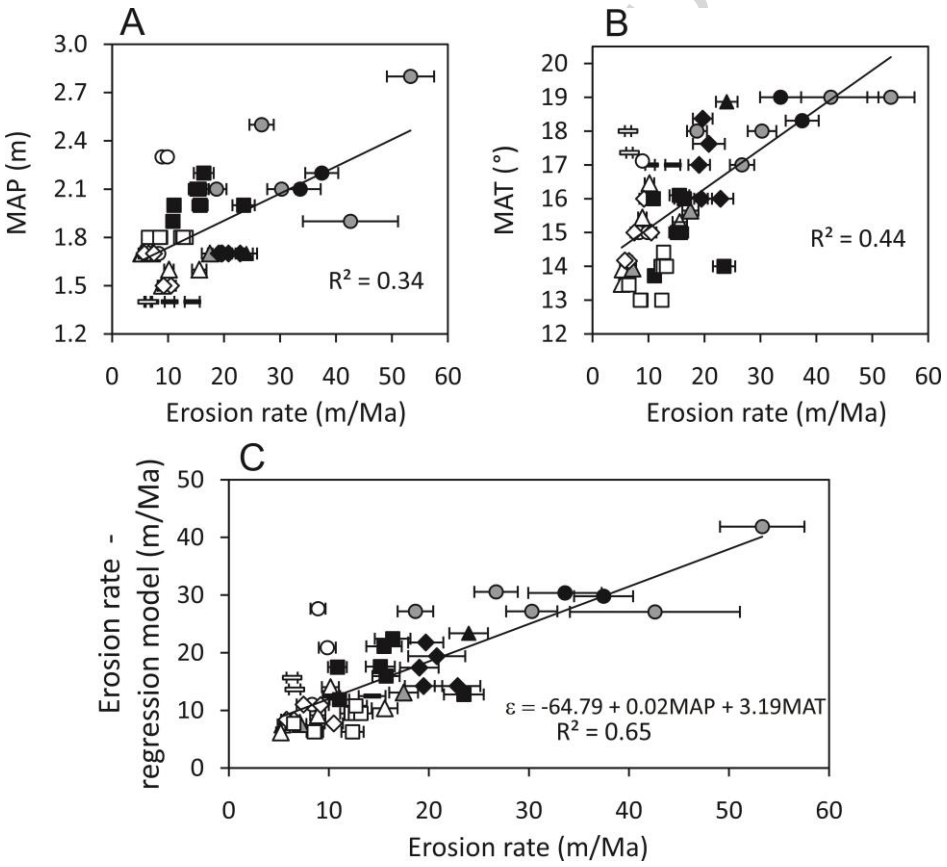

Figure 8

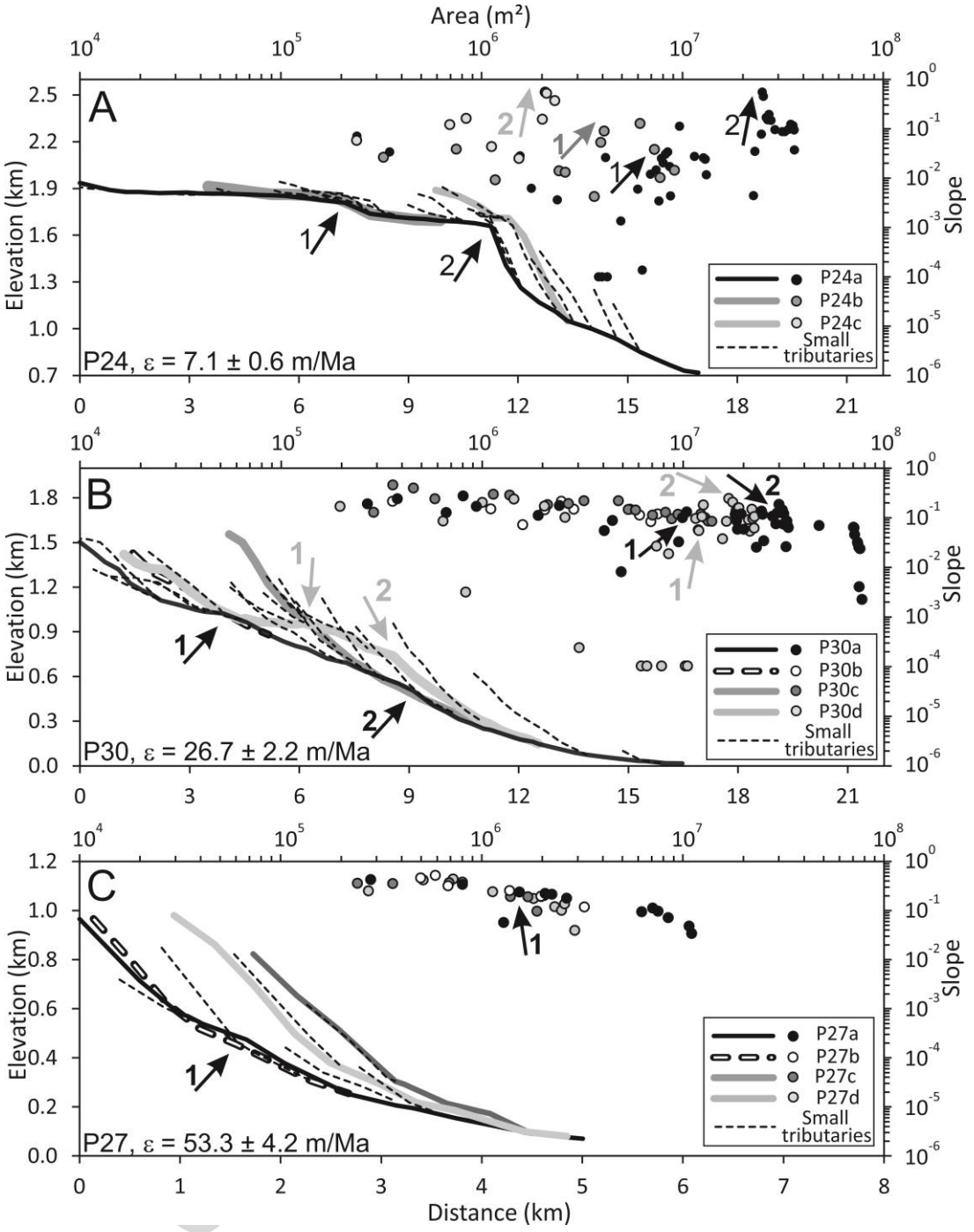

Figure 9

Tables

Table 1. Sample locations and ^{10}Be concentrations

Sample name	Latitude[1] (DD)	Longitude[1] (DD)	Elevation[2] (m)	Shielding correction[3]	^{10}Be concentration[4] (10^5atoms g^{-1})	Production rate[5] (atoms g^{-1} a^{-1}) Muons	Spallation
Campos do Jordão Plateau							
P18	-22.4427	-45.3377	1536	0.985	6.24 ± 0.15	0.124	8.71
P21	-22.5352	-45.4095	1303	0.984	4.74 ± 0.10	0.115	7.40
P6	-22.6937	-45.4926	1719	0.991	11.7 ± 0.23	0.131	9.99
P13	-22.5771	-45.3257	1752	0.989	11.57 ± 0.23	0.132	10.17
P20	-22.5365	-45.2572	1528	0.986	3.66 ± 0.09	0.123	8.69
P17	-22.7740	-45.4600	1432	0.973	3.07 ± 0.08	0.12	8.07
P23	-22.6125	-45.1479	892	0.977	1.61 ± 0.05	0.101	5.48
P24	-22.6650	-45.3061	1762	0.983	8.89 ± 0.21	0.133	10.20
Serra do Quebra-Cangalha							
P35	-22.9691	-45.3085	993	0.983	2.83 ± 0.14	0.104	5.98
P42	-22.8714	-45.1283	886	0.989	3.62 ± 0.09	0.101	5.55
P37	-22.9448	-45.0832	1035	0.996	6.07 ± 0.16	0.106	6.24
P38	-23.0138	-45.1567	1059	0.989	6.37 ± 0.18	0.107	6.32
Serra do Mar							
P26	-23.3470	-45.1369	1017	0.995	4.57 ± 0.11	0.105	6.22
P33	-23.1013	-44.8751	1424	0.988	6.28 ± 0.15	0.12	8.2
P34	-23.2040	-44.9777	1264	0.989	4.85 ± 0.14	0.114	7.35
P27	-23.3909	-45.1206	590	0.965	0.62 ± 0.02	0.092	4.41
P29	-23.0885	-44.7252	955	0.953	1.08 ± 0.03	0.103	5.65
P30	-23.2253	-44.7660	1011	0.972	1.58 ± 0.05	0.105	6.03

[1] Coordinates are from WGS84.

[2] Altitude corresponding to the average production rate in the basin according to Stone (2000) scaling from DEM.

[3] Average shielding factor in the basin calculated from DEM.

[4] ^{10}Be concentrations are based on ^{10}Be/Be ratio of $2.79 \cdot 10^{-11}$ for NIST SRM4325. The processed blank ratios ranged between 0.4 and 7.1 % of the sample ^{10}Be/Be ratios. Concentration uncertainties include AMS counting statistics and blank correction uncertainty.

[5] Production rates according to time-independent Lal/Stone scheme in CRONUS-Earth online calculators version 2.3 (Balco et al., 2008).

Concentrations reported by Salgado et al. (2016) are in Table S1.

Table 2. Catchments characteristics and ^{10}Be-derivated erosion rates.

Sample name	Catchment type[1]	Erosion rate[2] (m/Ma)	Apparent age[3] (ka)	Area (km²)	Slope[4] (°)	Local relief[4, 5] (m)	k_{sn} ($m^{0.9}$)[4] Drainage Area	k_{sn} ($m^{0.9}$)[4] Discharge[6]	Litho- type[7]	MAP[8] (mm)	MAT[9] (°C)
Campos do Jordão Plateau											
P18	H	8.9 ± 0.8	67	42	17	390	66	80	gn, grt	1500	15
P21	H	10.2 ± 0.8	59	27	18	386	55	68	gn, grt, sch	1600	16
P6	H	5.2 ± 0.5	116	12	16	274	37	48	grt, gn	1700	13
P13	H	5.4 ± 0.5	112	30	15	257	33	42	gn, grt	1700	14
P20	H	15.6 ± 1.3	39	48	17	342	37	46	gn, qtzt	1600	15
P17	M	17.5 ± 1.4	34	16	20	585	114	147	gn, sch, grt	1700	15
P23	E	24.9 ± 1.9	25	26	19	401	46	58	gn, sch	1700	19
P24	M	7.1 ± 0.6	84	35	16	336	77	98	grt, gn	1700	14
Serra do Quebra-Cangalha											
P35	E	14.3 ± 1.3	42	31	19	395	60	70	grt, gn, sch	1400	17
P42	E	10.3 ± 0.9	58	29	16	309	42	48	grt, gn, sch	1400	18
P37	H	6.6 ± 0.6	91	29	11	185	15	18	grt, sch, gn	1400	17

P38	H	6.3 ± 0.6	95	23	15	255	28	32	sch, gn, grt	1400	17
Serra do Mar											
P26	H	8.9 ± 0.7	67	25	12	186	10	14	gn, grt	2300	17
P33	H	8.3 ± 0.7	72	24	17	278	35	45	gn, grt, qtzt	1700	15
P34	H	9.8 ± 0.8	61	49	16	223	21	30	gn, qtzt	2300	15
P27	E	53.3 ± 4.2	11	13	24	618	109	162	gn	2800	19
P29	M	37.5 ± 3.0	16	31	24	631	115	157	gn, grt	2200	18
P30	M	26.7 ± 2.2	22	77	22	549	103	155	grt	2500	17
A1*	M	18.7 ± 1.8	32	10	21	541	109	151	gn	2100	18
A2*	M	30.3 ± 2.6	20	21	22	637	116	155	gn	2100	18
A3*	E	33.6 ± 3.7	18	16	23	662	119	160	gn, grt	2100	19
A4*	M	42.6 ± 8.5	14	14	22	638	104	139	gn, grt	1900	19
A5**	M	34.8 ± 22.2	17	38	21	540	104	137	gn	1900	18
Bocaina Plateau											
B1*	H	6.5 ± 0.6	92	8	16	307	25	32	sch, gn, grt	1700	14
B2*	H	5.8 ± 0.5	104	9	16	323	26	33	sch, gn, grt	1700	14
B3*	H	10.5 ± 0.9	57	45	18	368	50	60	sch, gn, grt	1500	15
B4*	H	7.5 ± 0.7	80	200	17	316	43	53	sch, gn, grt	1700	15
B5*	H	9.2 ± 0.8	65	14	18	316	31	38	grt, sch, gn	1500	16
C1*	E	22.9 ± 2.3	26	17	23	654	101	129	sch, gn	1700	16
C2*	E	19 ± 1.9	31	21	24	669	115	148	sch, gn, grt	1700	17
C3*	E	19.4 ± 1.9	31	21	25	622	93	119	sch, gn, grt	1700	16
C4*	E	20.8 ± 2.8	29	17	22	570	98	124	sch, gn	1700	18
C5*	E	19.7 ± 1.8	30	9	21	516	79	102	sch, gn, grt	1700	18
Itatiaia Plateau											
D1*	E	23.5 ± 2.0	26	10	21	506	87	118	grt	2000	14
D2*	E	11 ± 1.0	54	9	22	566	93	125	grt	2000	14
D3*	E	15.2 ± 1.4	40	24	21	521	87	118	grt	2100	15

D4*	E	15.7 ± 1.7	38	12	24	581	89	120	grt	2000	15
D5*	E	10.86 ± 0.9	55	23	22	504	72	95	grt	1900	16
D6*	E	16.9 ± 1.8	37	20	19	402	46	64	grt, gn	2200	16
D7*	E	15.5 ± 1.8	39	27	21	478	62	84	grt	2100	16
E1*	H	12.4 ± 1.1	49	10	17	395	57	74	grt	1800	13
E2*	H	6.5 ± 0.6	92	8	17	437	65	85	grt	1800	13
E3*	H	12.2 ± 1.1	49	22	18	407	65	85	grt	1800	14
E4*	H	8.6 ± 0.8	69	8	19	448	66	86	grt	1800	13
E5*	H	12.6 ± 1.1	47	25	21	508	75	98	grt	1800	14
E6*	H	8.5 ± 0.8	70	10	20	457	66	86	grt	1800	13
E7*	H	13.2 ± 1.2	45	28	21	511	74	96	grt	1800	14
E8*	H	12.7 ± 1.1	47	11	21	487	66	86	grt	1800	14

[1] Catchment type: escarpment (E), highland (H) and mixed (M).

[2] Erosion rates according to time-independent Lal/Stone scheme in CRONUS-Earth online calculators version 2.3 (Balco et al., 2008), ^{10}Be concentrations and production rates in table 1.

[3] Residence time in rock within one absorption depth scale according to von Blanckenburg (2005).

[4] All morphometric parameters were extracted from 30 m DEM SRTM.

[5] Circular moving window with 1 km radius, results for other radii are shown in Table S2.

[6] K_{sn} calculated by replacing in equation 1 drainage area with discharge, which was calculated from the MAP.

[7] Nomenclature: (gn) gneiss; (grt) granite; (sch) schist; (qtz) quartzite. See Supplementary Data 2D.

[8] (MAP) Mean annual precipitation

[9] (MAT) Mean annual temperature

* Calculated from the ^{10}Be concentrations published by Salgado *et al.* (2016), see Table S1.

** We excluded the A5 of the analysis given its anomalous high analytical error.

HIGHLIGHTS

- ^{10}Be-derived catchments mean erosion rates in the ocean-facing coastal escarpment catchments of the Serra do Mar (ε = 18–53 m/Ma) are approximately twice higher than continent-facing escarpment catchments (ε = 7–24 m/Ma).
- Geomorphic metrics for river incision and hillslope erosion processes are correlated each other and approach threshold values in the high-relief escarpment areas, mainly in Serra do Mar.
- Episodic river captures as recorded in the mixed topography catchments results in the dissection of the low-relief highlands and the excavation and migration of escarpments inland.
- Precipitation-temperature gradient is well correlated with erosion rates and explain the higher erosion rates in the coastal escarpment catchments of the Serra do Mar.